Cancer Nanotechnology

RESEARCH

Open Access

High-frequency ultrasound-assisted drug delivery of chia, cress, and flax conjugated hematite iron oxide nanoparticle for sono-photodynamic lung cancer treatment in vitro and in vivo

Samir Ali Abd El-Kaream[1], Doha Farhat Mohamed Zedan[2], Hagar Mohamed Mohamed[1,4], Amal Saleh Mohamed Soliman[3], Sohier Mahmoud El-Kholey[2] and Mohammed Kamal El-Dein Nasra[2*]

*Correspondence:
Mohamednasrakmri@gmail.com

[1] Applied Medical Chemistry Department, Affiliated Medical Research Institute, Alexandria University, Alexandria, Egypt
[2] Medical Biophysics Department, Affiliated Medical Research Institute, Alexandria University, Alexandria, Egypt
[3] Basic Science Department, Affiliated Alexandria Higher Institute for Engineering and Technology, AIET, Alexandria, Egypt
[4] Medical Laboratory Analysis Department, Affiliated Faculty of Medical & Health Sciences, Liwa College, Abu Dhabi, United Arab Emirates

Abstract

Background: Sono-photodynamic therapy (SPDT), which combines photodynamic (PDT) and sonodynamic (SDT) therapies with sensitizers, offers new avenues for cancer treatment. Even though new sensitizers for SPDT have been synthesized with great success, few of them are effectively used. The limited tumor-targeting specificity, inability to transport the sensitizers deeply intratumorally, and the deteriorating tumor microenvironment limit their anti-tumor effectiveness. The current study was carried out aiming at high-frequency ultrasound-assisted drug delivery of chia, cress and flax conjugated hematite iron oxide nanoparticles (CCF–HIONP) for photothermal–photodynamic lung cancer (LCA) treatment in vitro and in vivo as activated cancer treatment up-to-date modality.

Materials and methods: The study was conducted in vitro on human LCA cells (A-549) and the study protocol application groups in vivo on Swiss albino mice treated with benzo[a]pyrene only and were not received any treatment for inducing LCA, and only after LCA induction the study treatment protocol began, treatment was daily with CCF–HIONP as HIFU–SPDT sensitizer with or without exposure to laser (IRL) or high-frequency ultrasound (HIFU–US) or a combination of laser and/or high-frequency ultrasound for 3 min for 2 weeks.

Results: Revealed that HIONP can be employed as effective CCF delivery system that directly targets LCA cells. In addition, CCF–HIONP is a promising HIFU–SPS for HIFU–SPDT and when combined with HIFU–SPDT can be very effective in treatment of LCA–A549 in vitro (cell viability decreased in a dose-dependent basis, the cell cycle progression in G0/G1 was slowed down, and cell death was induced as evidenced by an increase in the population of Pre-G cells, an increase in early and late apoptosis and necrosis, and an increase in autophagic cell death) and benzo[a]pyrene LCA-induce mice in vivo (decreased oxidative stress (MDA), and ameliorated enzymatic and non-enzymatic antioxidants (SOD, GR, GPx, GST, CAT, GSH, and TAC) as well

as renal (urea, creatinine) and hepatic (ALT, AST) functions, induced antiproliferative genes (caspase 3,9, p53, Bax, TNFalpha), suppressed antiapoptotic and antiangiogenic genes (Bcl2,VEGF respectively) and effectively reducing the growth of tumors and even leading to cancer cell death. This process could be attributed to photochemical and/or high-frequency sono-chemical activation mechanism HIFU–SPDT.

Conclusions: The results indicate that CCF–HIONP has great promise as an innovative, effective delivery system for selective localized treatment of lung cancer that is activated by HIFU–SPDT.

Keywords: Lung cancer, Hematite nanoparticle, Chia, Cress, Flax, Sono-Photodynamic

Introduction

Lung cancer (LCA) ranks fifth for both men and women in Egypt and is the second most common cancer globally, as well as ranking 1st and 4th among the top cancer-related deaths worldwide and Egypt respectively. It accounts for 18.4% of all cancer-related fatalities globally, making it the primary cause of cancer death (Bray et al. 2018). Five years after diagnosis, just 15% of LCA patients remain alive, with 70% of patients having advanced illness at that point (Siegel et al. 2018). There are several methods available for diagnosing LCA. The most common imaging technique for determining the location and size of lung tumors, accurately staging the disease, and identifying ambiguous lung nodules is a combined PET–CT scan (Rivera et al. 2013; Hochhegger et al. 2015). For the best possible treatment of lung malignancies, an effective therapeutic approach is required in addition to early diagnosis. The patient's functional status, the stage, and the histological type of the cancer all influence the best course of treatment for LCA. LCA is typically treated with a variety of therapeutic techniques, such as immunotherapy, chemotherapy, radiation, and radiosurgery. However, the limitations of each form of treatment pose challenging issues for LCA therapy. A thorough investigation and the development of novel treatments for malignant tumors can improve the overall survival rate of LCA patients. Furthermore, the cytotoxicity of chemotherapy medications and conventional cancer therapies causes unfavorable side effects and an inability to control the cancerous condition (Kozower et al. 2013; Ko et al. 2018; Carrasco-Esteban et al. 2021).

An alternate tactic to mitigate the harmful effects of synthetic chemicals is to employ medicinal plants. Furthermore, cutting-edge methods for treating malignant tumors are being actively studied and developed, which enhances patient survival in general. High-frequency sono-photo-dynamic therapy (HIFU–SPDT) is one of the LCA alternative therapeutic approaches that uses photo-irradiation of the tumor in addition to high-frequency sonography and sensitizer to treat the disease. In recent years, HIFU–SPDT has become more and more popular as a means of treating different tumors, either on its own or in combination with other forms of therapy. In HIFU–SPDT, a high-frequency sono-photo-sensitizing (HIFU–SPS) is applied, and the malignant region is subsequently exposed to high-frequency ultrasound and light that has the same absorbance wavelength as the HIFU–SPS. This combination of treatments triggers a variety of biological processes. The application of HIFU–SPSs plant-based therapeutic substances provides an alternative to the deleterious effects of synthetic drugs. Few researches have concentrated on phytochemicals obtained

from plants; instead, most studies have examined the biochemical consequences of phytochemicals produced from plants (Rengeng et al. 2017; Shen et al. 2018; Szasz 2019; Abd El-Kaream et al. 2018; Abd El-Kaream 2019; Qiu et al. 2022).

Even though they are small, seeds have enormous advantages. Similar to nuts, seeds have a plethora of health advantages. They resemble these little, nutrient-dense powerhouses with more to provide than can be imagined. Seeds are nutritious and a fantastic source of minerals, zinc, protein, and other elements that can prolong one's life. There are seeds everywhere, changing the way people thinks about health and where they should be in their diets. *Salvia hispanica*, or chia, seeds are some of the world's healthiest foods. They are a common ingredient in energy bars since they are rich in nutrients that are vital for the body, brain, and energy production. They are bursting with antioxidants that guard against cancer, ageing, and bad cholesterol. By slowing the rise in blood sugar, they aid with diabetes. Chia seeds are a great source of calcium, omega 3, and protein. They support weight loss as well. Garden cress, *Lepidium sativum,* seeds are an excellent remedy for anemia because of their high iron and folic acid content. They are recognized to help women's menstrual cycles become more regular and are high in phytochemicals. These little brown seeds not only support the health of women but also assist control blood sugar, shield the liver, ease gastrointestinal discomfort, and prevent cancer. *Linum usitatissimum*, or flax, seeds can be found in a wide variety of meals, including energy bars and crackers. They are abundant in fiber, protein, and omega 3. These incredibly tiny seeds have nearly endless health benefits, including avoiding cancer, protecting your heart, and curing both constipation and diarrhea. These seeds' ability to decrease blood cholesterol is their main medicinal use. In addition, flax seeds assist diabetics in controlling their blood pressure and blood sugar levels (Abd El-Kaream 2019; Sanlier and Guler 2018; Soundararajan and Kim 2018; Kulczyński et al. 2019; Azene et al. 2022; Merkher et al. 2023).

It has not been thoroughly investigated how chia, cress and flax conjugated hematite iron oxide nanoparticles (CCF–HIONP) works as anticancer or how it could be applied to HIFU–SPDT as an HIFU–SPS. Consequently, the main objective of the present work is to offer a novel investigation to assess the high-frequency ultrasound-assisted drug delivery of chia, cress and flax conjugated hematite iron oxide nanoparticles for high-frequency sono-photo-dynamic cancer treatment in vitro and in vivo.

Materials and methods

Materials

Every chemical utilized came from a commercial source and didn't require any additional purification. Ferric chloride hexahydrate and sodium hydroxide ($FeCl_3.6H_2O$, NaOH respectively) were obtained from (Sigma-Aldrich). Chia, cress and flax were obtained from Aladdin Industries Inc. (Shanghai, China).Kits of (TAC), catalase (CAT), total antioxidant capacity, glutathione-S-transferase, peroxidase and reductase (GST, GPx, GSR), Superoxide dismutase (SOD), aspartate, alanine aminotransferase (ALT, AST), urea and creatinine, were acquired from Cairo Biodiagnostic, Egypt, along with lipid peroxide (Malondialdehyde; MDA). The ABT (spin column) total RNA Mini extraction kit, ABT cDNA H-minus synthesis kit, and WizPure™ qPCR (SYBR) Master were acquired from Wizbiosolutions Inc. and Applied Biotechnology, respectively.

Preparation and characterization of CCF–HIONP

CCF–HIONP was utilized as HIFU–SPS in the current work. Hematite iron oxide nanoparticle (HIONP) synthesis procedures, creating a 0.22M solution, 7 mmol of $FeCl_3.6H_2O$ were dissolved in deionized water. 21 mmol of NaOH solution was added dropwise to this solution at room temperature while being stirred magnetically. When the $FeCl_3.6H_2O$ solution and the NaOH solution had thoroughly mixed, a brownish suspension had formed. Without any extra equipment, the mixture was put into a basic microwave reactor system and heated for 15 min at 500W of electricity. After the heating in the microwave, red suspension was obtained. The suspension was then calcined for 15 min at 350 degrees Celsius (ºC) using a straightforward heating technique. The sample was naturally cooled to room temperature before being twice cleaned with deionized water and alcohol, in that order. The sample was eventually dried in air at 110 °C to produce a reddish powder. Chia, cress and flax conjugated hematite iron oxide nanoparticle (CCF–HIONP) was prepared as following; creating a homogeneous dispersion, 250 mg of HIONP nanoparticles were sonicated in 500 ml deionized water for 30 min. Chia, cress, and flax (CCF) extract in 50 ml of aqueous sterilized buffer solution with a pH of 7.4 was then added to the mixture, and it was agitated for 24 h at room temperature. Next, for a whole day, the entire system was dialyzed against deionized water (Abd El-Kaream et al. 2018; Nurhayati et al. 2013). CCF–HIONP, and it was evaluated by means of scanning photoluminescence and absorbance spectrometry (PL, UV/Visible), Fourier transform infrared scanning spectroscopy (FTIR), scanning diffraction and energy dispersive X-ray (XRD, EDX), and transmission and scanning electron microscope (TEM, SEM) for measuring its dimensions. All CCF–HIONP treated LCA–A549 cell lines and the benzo[a]pyrene LCA-induced mice group (injected intraperitoneally; ip) CCF–HIONP allowed to incubate for 9–12 h prior to being exposed to PDT and/or HIFU–SDT, (Fig. 1).

Methods

All applicable regulations and standards were adhered to during the entire investigation whole inquiry process.

Ethics statement

The Animal Care and Use Institutional Committee of University granted its certification of ethical guidelines and standards of the animal protocol.

In vitro study: 1. (+ve Control): LCA cell line (A549) was maintained in drug-free environment and were kept without treatment. 2. (CCF–HIONP without activation group): LCA cell line (A549) was treated with 0.025 µl CCF–HIONP (dissolved in PBS) only. 3. (Laser group): LCA cell line (A549) was exposed to laser, for 3 min. 4. (CCF–HIONP laser activated group): LCA cell line (A549) was treated with 0.025 µl CCF–HIONP and exposed to laser as group 3. 5. (high-frequency ultrasound group): LCA cell line (A549) was exposed to high-frequency ultrasound for 3 min. 6. (CCF–HIONP high-frequency ultrasound activated group): LCA cell line (A549) was treated with 0.025 µl CCF–HIONP and exposed to high-frequency ultrasound as group 5. 7. (Laser and high-frequency ultrasound combined group): LCA cell line (A549) was exposed laser and

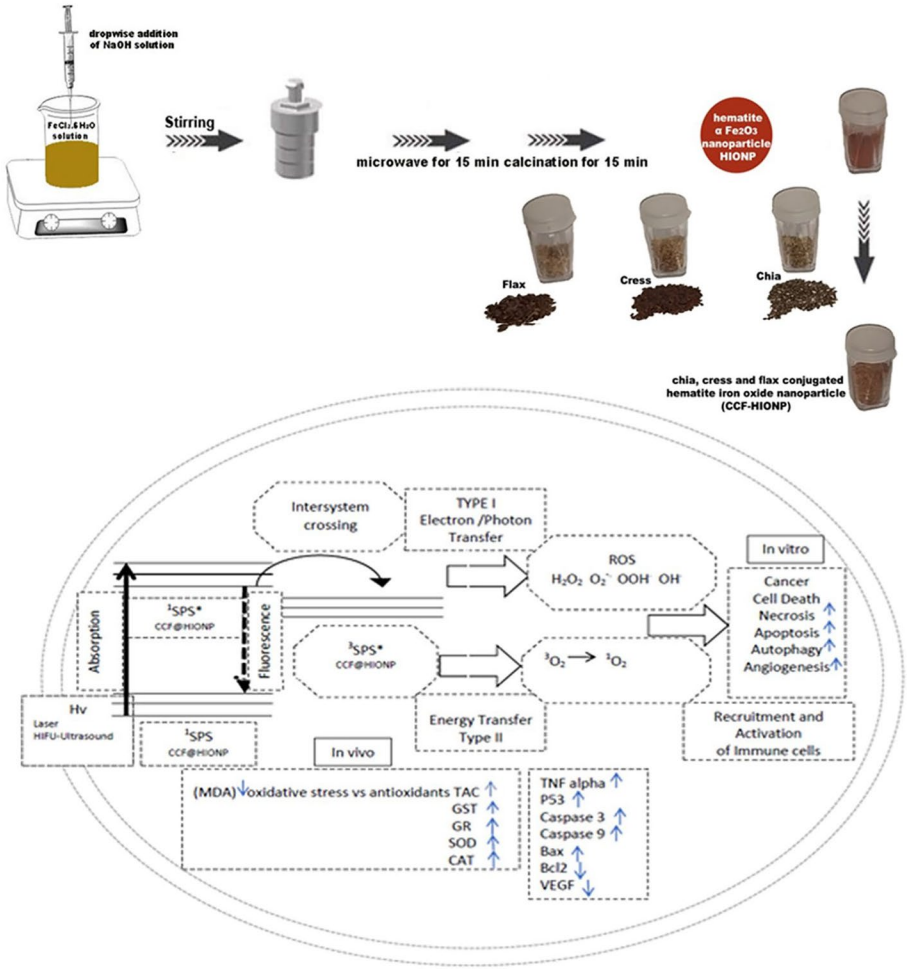

Fig. 1 Schematic representation of CCF@HIONP synthesis and HIFU-SPDT

high-frequency ultrasound for 3 min. 8. (CCF–HIONP laser and high-frequency ultrasound combined activated group): LCA cell line (A549) was treated with 0.025 µl CCF–HIONP, exposed to laser and high-frequency ultrasound as group 7.

In vivo study: Ninety Albino mice, with a weight range of 20 ± 5 g and of 60 ± 5 days, were acquired from the animal house. Mice were housed in appropriate cages with twelve wake-light/sleep-dark cycles and an ambient temperature of 25 ± 0.5 °C. The mice had unrestricted access to tap water and were fed a regular, consistent pellet diet. The medication was started after a week of acclimation for the mice. In summary, the mice were divided into nine groups of ten mice each: 1 (Negative Control group): Untreated normal, healthy mice were maintained. 2 (Positive LCA Control group): mice were received 100 mg/kg bw/once benzo[a]pyrene only to induce LCA and maintained without treatment. 3 (CCF–HIONP without activation group): LCA induced mice were treated by a daily dose of 0.025 ml of dissolved CCF–HIONP in PBS only. 4 (Laser exposed group): For 2 weeks, LCA-induced mice were subjected to laser for 3 min every day. 5 (Laser activated CCF–HIONP group): LCA induced mice were treated by a daily dose of 0.025 ml of CCF–HIONP per mouse and subsequently subjected to a laser

for 3 min every day. 6 (High-frequency ultrasound exposed group): For 2 weeks, LCA-induced mice were subjected to high-frequency ultrasound for 3 min each day. 7 (High-frequency ultrasound activated CCF–HIONP group): LCA-induced mice were treated by a daily dose of 0.025 ml of CCF–HIONP per mouse and subsequently subjected to high-frequency ultrasound for 3 min every day. 8 (Laser and high-frequency ultrasound combination activated group): For 2 weeks, LCA-induced mice were subjected to laser light, then high-frequency ultrasound for 3 min every day. 9 (Laser and high-frequency ultrasound combined activated CCF–HIONP group): LCA-induced mice were treated by a daily dose of 0.025 ml CCF–HIONP per mouse, and were exposed to both laser and high-frequency ultrasound for 3 min each day.

Instruments

Laser irradiation

The mice were made anesthetic with 100 mg/kg bw Ketamine and 10 mg/kg bw Xylazine injection before to the laser exposure. The hair was shaved around the tumor. The mouse was placed with its back to the board. The probe was positioned almost atop the tumor exactly, and each group received a 3-min laser therapy under the predetermined conditions. After PDT, to prevent skin irritation mice were maintained in the dark. A laser type LAS 250-Hi-Tech infrared diode, fysiomed, China, with a peak 50 W output and a 600–904 nm wavelength of 7000 Hz frequencies, was utilized to expose the tumor in mice (10 mW and 0.43 J/cm2).

Ultrasound irradiation

The mice were made anesthetic with 100 and 10 mg/kg bw Ketamine, Xylazine respectively injection before to the ultrasound exposure. The hair was shaved around the tumor. The mouse was placed with its back to the board. The probe was positioned almost atop the tumor exactly, and each group received a 3-min ultrasound therapy under the predetermined conditions. The tumor in the mice was exposed by means of an ultrasonic (Shanghai, CSl China, Model 822), which generates an alternating electric current oscillation at a 0.8 MHz frequency using an electronic tube. An ultrasonic transducer is used to transform the device's power output into mechanical ultrasonic energy MUSE. Ultrasonic mechanical energy has a power beam density that ranges from 0.5 to 3 W/cm^2. With an output power range of 0.5–3 W/cm^2 (pulse 1000 Hz frequency, duty 1/3 ratio, and power density average 0.15–1 W/cm2 range), this device can work in both pulsed and continuous modes.

When the study protocol was over, the mice were euthanized by inhaling 5% (overdose) isofurane and immediately after 60 s as the animals no longer have a heartbeat and have whitish eyes, cervical dislocation was performed to ensure euthanasia. After the dissection, blood samples were taken in order to get whole blood and sera. One portion of the blood was centrifuged for 10 min at 1000xg, and the separated sera were kept until analysis at − 20 °C. The leftover blood sample was collected and maintained until the analysis of genes relative expressions identification was initiated at − 80 °C. It was then transferred from the vial containing EDTA to another vial containing RNA later solution. In addition, LCA tissues were taken out right away, cleaned in cold saline, pierced in a vial with a needle, and kept for histological analysis in 10% formalin/saline.

Cell culture

Lung adenocarcinoma human cell A549 was provided from the American Type Culture Collection (ATCC). The cells were cultured at 37 °C in a humidified 5% (v/v) CO_2 environment in DMEM medium supplemented with 10% heat-inactivated fetal bovine serum, 100 mg/mL streptomycin, and100 units/mL penicillin.

Assay for cytotoxicity and cell viability

The cytotoxic effect of CCF–HIONP against A549 cells was assessed using the sulforhodamine B (SRB) test. After aliquots of 100 µL (5×10^3 cells) cell suspension were planted on 96-well plates, the entire medium was incubated for 24 h. The cells were further treated with aliquot of 100 µL media with CCF–HIONP at various doses (1000, 100, 10, 1.0, and 0.1 µM).After being exposed to various modalities for 24 h, with and without CCF–HIONP, the cells were fixed by replacing the media with 150 µL of 10% TCA and incubated for 1 h at 4 °C. Following the removal of the TCA solution, the cells were washed with distilled water five times. Aliquots of 70 µL (0.4% w/v) SRB solution were added, and they were then left to sit in a dark place at room temperature for 10 min. The plates were allowed to air dry for the full night following three washing with 1% acetic acid. The SRB protein-bound stain was then dissolved with 150 µL of (10 mM) TRIS, and the absorbance at 540 nm was measured using a LABTECH®-FLUOstar BMG Omega microplate reader (Ortenberg, Germany) (Vichai and Kirtikara 2006).

Flow cytometry assay

Cell cycle analysis

After being treated with different modalities for 24 h, both with and without CCF–HIONP, A549cells (10^5 cells) by trypsinization were collected. After that, the cells were twice cleaned in ice-cold (pH 7.4) PBS. The cells were fixed for an hour at 4 °C after being re-suspended in two milliliters of 60% ice-cold ethanol. The fixed cells were first suspended in 1 mL of PBS with 10 µg/mL propidium iodide (PI) and 50 µg/mL RNAase A, and then they were repeatedly washed in PBS (pH 7.4). After incubating in the dark for 20 min at 37 °C, the cells were analyzed by flowcytometry using an ACEA Novocyte™ flowcytometer (ACEA Biosciences Inc., CA, San Diego, USA) equipped with a FL2 (λex/em 535/617 nm) signal detector to ascertain the DNA content of the cells. For every sample, a total of 12,000 events were collected. The cell cycle distribution was ascertained using NovoExpress™ ACEA software (ACEA Biosciences Inc., CA, San Diego, USA) (Pozarowski and Darzynkiewicz 2004).

Analysis of necrosis and apoptosis in Annexin V-FITC/PI

The populations of necrosis and apoptosis cells were identified using two fluorescent channels flowcytometry in combination with the Abcam Inc., Science Park, Cambridge, UK, Annexin V-FITC apoptosis detection kit. Following a 24-h period of treatment with various modalities both with and without CCF–HIONP, A549 cells (10^5 total) were isolated using trypsinization and twice washed in pH 7.4 ice-cold PBS. Cells were treated with 0.5 ml of Annexin V-FITC/PI solution for 30 min in the dark

at room temperature, as per the manufacturer's instructions. Following staining, the fluorescence signals for FITC and PI were evaluated using FL1 and FL2 signal detectors (λex/em 488/530 nm and 535/617 nm for FITC and PI respectively), respectively, using NovocyteTM ACEA flowcytometer. For each sample, a total of 12,000 events were recorded. Positive FITC and/or PI cells were computed and quantified using quadrant analysis using NovoExpress™ ACEA software (Wlodkowic et al. 2009).

Autophagy analysis

Acridine orange (AO), a lysosomal dye, and flowcytometric analysis were used to quantify autophagic cell death. Trypsinization was used to extract A549 cells (10^5 cells) after different modalities were used for 24 h, both with and without CCF–HIONP. After that, the cells were twice cleaned in ice-cold PBS (pH 7.4). The cells with (10 μM) acridine orange were stained and then incubated at 37 °C in the dark for 30 min. After labeling, cells were injected using an ACEA Novocyte™ flowcytometer, and the fluorescent acridine orange signals were analyzed using the FL1 (λex/em 488/530 nm) signal detector. For each sample, 12,000 events were gathered, and net fluorescence intensities (NFI) are measured using NovoExpress™ ACEA software (Thomé et al. 2016).

Migration (Wound healing) assay

Using a cell scratch assay, the effect of CCF–HIONP on A549 cell migration was examined. A549cells were seeded onto a coated 12-well plate at a density of 2×10^5/well for the wound scratch assay. After that, they were grown in 5% FBS–DMEM for the whole night at 37 °C and 5% CO2. The next day, scratches horizontally were applied to the confluent monolayer. After that, PBS was used to thoroughly clean the plate. New media containing activated CCF–HIONP was added to the treatment wells, and fresh medium was added to the control wells. At predetermined intervals, pictures were taken with an inverted microscope. The plate was incubated with 5% CO_2 in between time intervals at 37 °C. Version 3.7 of the MII ImageView program displays and analyses the obtained images (Justus et al. 2014).

Histological, molecular, and biochemical analyses

Examination of the Liver and Kidney Enzymes Biochemically

Using commercial kits, kidney (creatinine, and urea) and the liver (AST, and ALT) enzymes were tested in accordance with Burtis et al. (2008).

Determination of the antioxidant markers and oxidative stress (oxidants)

The levels of antioxidant markers and oxidants in the serum were assessed using commercial kits. malondialdehyde (MDA), which are implied to predicting lipid peroxidation (Draper and Hadley 1990). SOD activity (Marklund and Marklund 1974). Glutathione-S-transferase, peroxidase and reductase (GST, GPx, GR) activities (Habing et al. 1974). Catalase activity (Aebi 1984). Total antioxidant activity (TAC) (Rice-Evans and Miller 1994).

Evaluation of Caspase (3, 9), p53, TNF alpha, Bax, Bcl-2, and VEGF relative gene expressions

qRT–PCR was used to determine genes expressions. Total RNA from blood samples was isolated using the Total RNA ABT extraction Mini column spin kit according to the directions. Purity by measuring the absorption 260/280 nm ratio was determined, which was usually greater than 1.8. As directed by the cDNA synthesis ABT H-minus kit, the cDNA was produced using an RT–PCR one-step reaction. For qRT–PCR, qPCR Master WizPure™ (SYBR) with ROX Dye was utilized. A reaction (20 µL) mixture using the template (5 µL) C-DNA and target gene primers (0.25 µM) P53-R: TGG AATCAACCCACAGCTGCA, CTGTCATCTTCTGTCCCTTC is P53-F, Caspase3-R: AAATGACCCCTTCATCACCA, TGTCATCTCGCTCTGGTACG is Caspase3-F, Caspase9-F: AGTTCCCGGGTGCTGTCTAT, GCCATGGTCTTTCTGCTCAC is Caspase9-R, TNF-α-R: TGAGATCCATGCCGTTGGC, CACGTCGTAGCAAAC CACC is TNF-α-F: Bax-R: CCAGTTCATCTCCAATTCG, CTACAGGGTTTCATC CAG is Bax-F, Bcl2-F: GTGGATGACTGAGTACCT. CCAGGAGAAATCAAACAG AG is Bcl2-R, VEGF-R: TTTCTCCGCTCTGAACAAGG, AAAAACGAAAGCGCA AGAAA is VEGF-F, using qRT–PCR Sybr Green (10 µL) and β-actin-R (CTCTCA GCTGTGGTGGTGAA) and β-actin-F (AGCCATGTACGTAGCCATCC) was utilized. 35 cycles were employed in each run of PikoReal Thermo Scientific's qRT–PCR apparatus (PR0241401024), with 10 s at 95 °C, 10 s at 55 °C, and 5 s at 72 °C. The initial denaturation was done for 5 min at 95 °C. The identical sample β-actin mRNA levels were used to compare all of the gene expressions, and the fold difference was calculated using the Eq. $2^{-\Delta\Delta Ct}$ previously mentioned (Abu Rakhey et al. 2022).

LCA tissue histopathology analyses

After being embedded in paraffin, the gathered LCA samples were sectioned into sections after being fixed by soaking them in a formalin/saline (10%) solution. To ascertain the extent of the histological changes in the LCA tissue, eosin and hematoxylin (H&E) staining dye was used. Every slide was inspected and photographed using a light microscope (Hu et al. 2021).

For statistical analysis

The data as mean ± standard deviation (SD) was given. One-way analysis of variance (ANOVA) was applied to confirm the statistical variances of the data. To establish statistical significance, p value of less than 0.05 was utilized. To compare groups, SPSS 25.0's post hoc analysis function was utilized.

Results

Characterization of CCF–HIONP

According to XRD/EDX crystallinity and purity nature, PL photoluminescence peak, optimal UV–Vis absorption peak, FTIR bands obtained corresponding to the functional groups respective vibrations present in CCF–HIONP, as well as the shape and

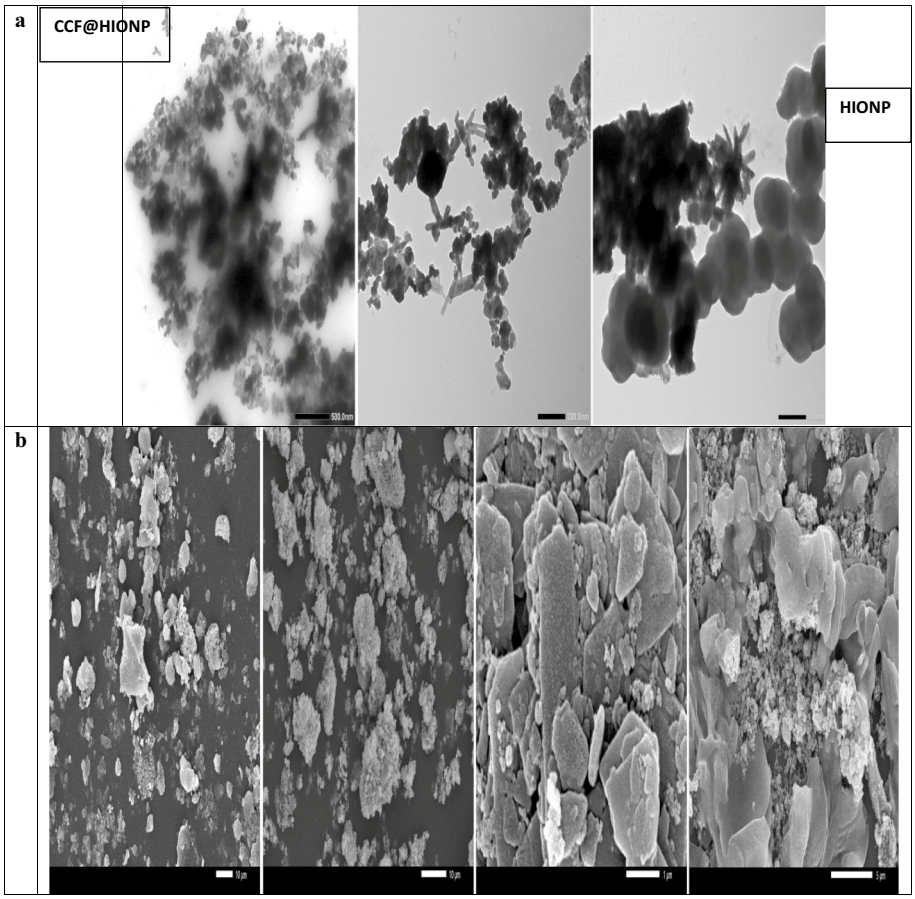

Fig. 2 Characterization of CCF@HIONP; **a** TEM, **b** SEM **c** particle size, **d** zeta potential of CCF@HIONP, **e** UV–vis spectra, **f** PL, **g** FTIR absorbance and transmittance, **h** XRD of (1. CCF@HIONP, 2. chia, 3. cress, 4. flax), **i** EDX of CCF@HIONP

size by particle size analyzer, TEM and SEM and zeta potential Fig. 2, all indicated that CCF–HIONP was successfully synthesized in accordance with previous studies.

Cytotoxicity of PDT, HIFU–SDT and HIFU–SPDT in presence and absence of (CCF–HIONP) upon treatment of LCA A549 cell line

The cytotoxic effect of different activation modalities with and without CCF–HIONP was investigated in LCA A549 cells after 24 h treatments using the SRB viability assay. The LCA A549 cell line underwent treatment with varying CCF–HIONP doses and different activation modalities, which led to an elevation in the number of floating cells and a change in cellular morphology. In addition, the SRB test was applied to asses PDT, HIFU–SDT, and HIFU–SPDT in the presence and absence of CCF–HIONP cytotoxicity, the results showed that the CCF–HIONP reduced LCA A549 cell proliferation in a dose-responsive manner. In addition, the cytotoxicity analysis findings of the current work manifested that the LCA A549 cell line was slightly affected by treatment with CCF–HIONP without activation followed by the LCA A549 cell line treated with lasers, high-frequency ultrasound without CCF–HIONP. The LCA A549 cells cytotoxic effectiveness and growth inhibition owing to laser (PDT) and the high-frequency ultrasound

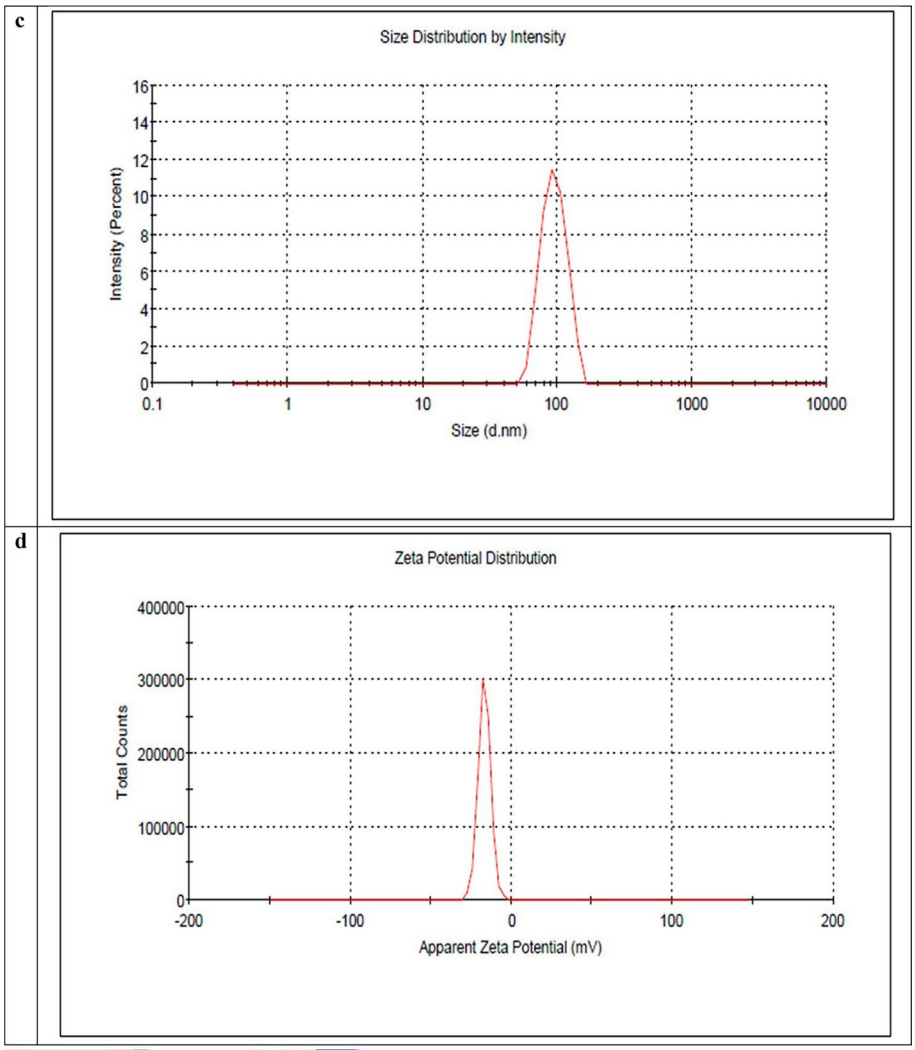

Fig. 2 continued

(HIFU–SDT) are both improved by the presence of CCF–HIONP. The acquired results demonstrated that both with and without the CCF–HIONP, HIFU–US is more cytotoxic effective than laser against LCA A549 cell line. For integration with laser, high-frequency ultrasound was chosen. In comparison to employing IRL or HIFU–US alone, the combination therapy approach (HIFU–SPDT) in presence of CCF–HIONP is most cytotoxic effective against LCA A549 cell line. Plotting cell viability vs. concentration yielded the CCF–HIONP that inhibits of the viable cells 50% (IC50), which was determined in μg/mL Fig. 3a.

Cell cycle distribution effect of PDT, HF-SDT and HF-SPDT in presence and absence of (CCF–HIONP) upon treatment of LCA A549

When LCA A549 cells are treated with CCF–HIONP at an IC50 equivalent concentration, a rise in the cell population at the G1 phase has been observed. The LCA A549 cell line was slightly affected by treatment with CCF–HIONP without activation exhibited

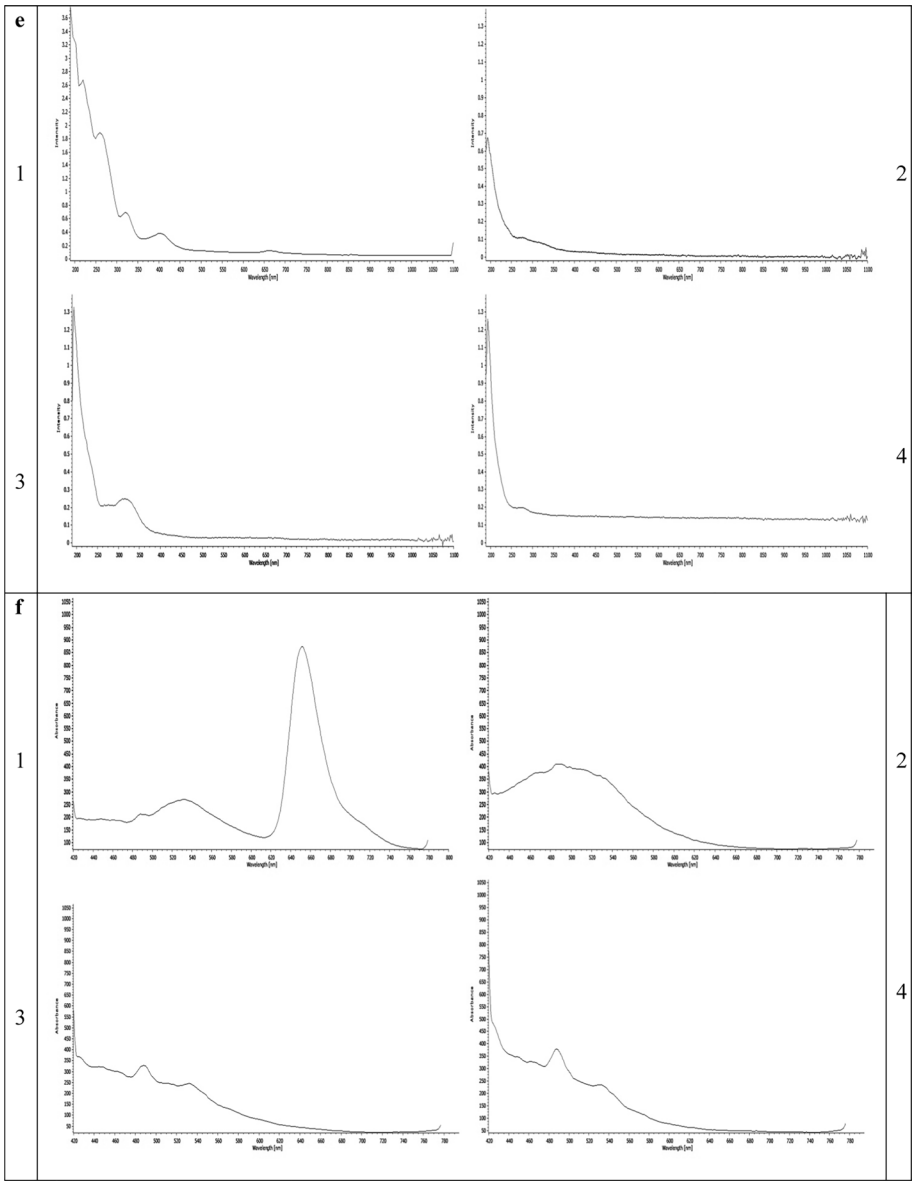

Fig. 2 continued

increase in the cell population at the G1 phase and resulted in cell death manifested by increase in the Sub G1 phase and reciprocally, caused a decline in the S phase and G2/M phase followed by the LCA A549 cell line treated with lasers, high-frequency ultrasound without CCF–HIONP. The effectiveness LCA A549 cells distribution, arrest and growth inhibition owing to laser (PDT) and the high-frequency ultrasound (HIFU–SDT) are both improved by the presence of CCF–HIONP exhibited increase in the cell population at the G1 phase and resulted in cell death manifested by increase in the Sub G1 phase and reciprocally, caused a decline in the S phase and G2/M phase. The acquired results demonstrated that both with and without the CCF–HIONP, HIFU–US is more effective than IRL against LCA A549 cell line. For integration with laser, high-frequency ultrasound was chosen. In comparison to employing IRL or HIFU–US alone,

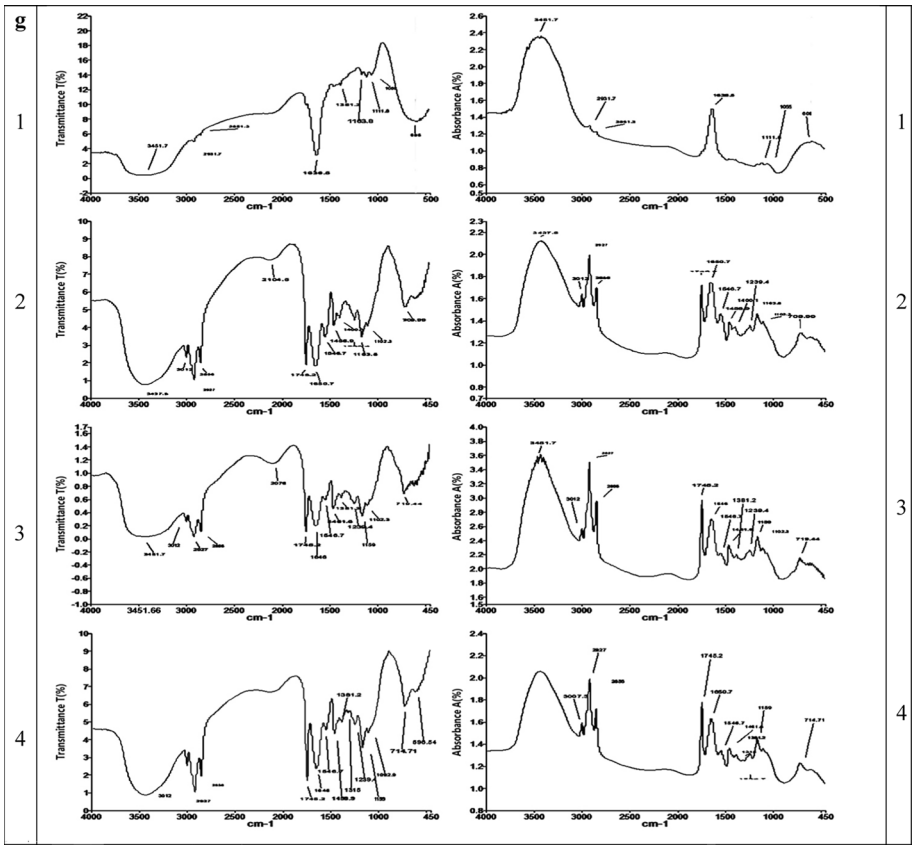

Fig. 2 continued

the combination therapy approach (HIFU–SPDT) in presence of CCF–HIONP is most effective against LCA A549 cell line exhibited increase in the cell population at the G1 phase and resulted in cell death manifested by increase in the Sub G1 phase and reciprocally, caused a decline in the S phase and G2/M phase Fig. 3b.

Apoptosis and necrosis cell death mechanism of PDT, HIFU–SDT and HIFU–SPDT in presence and absence of (CCF–HIONP) upon treatment of LCA A549

The SRB test and microscopic examination point to an apoptotic reaction to CCF–HIONP as the possible cause of the decrease in cell viability. In order to gain additional insight into the process of cell death (apoptosis versus necrosis), LCA A549 cells with different activation modalities were treated in presence and absence of CCF–HIONP for 24 h. The flowcytometric histogram of the treated cells showed a progressive population shift from the (living cells) left lower quadrant to the (early apoptosis) right lower one, then from the (late apoptosis) upper right to the (cell necrosis) upper left. The treated cells also showed increase of annexin V positivity. LCA A549 cells treated with either CCF–HIONP without activation or with lasers and high-frequency ultrasound without CCF–HIONP showed a substantial increase in the proportion of cells exhibiting early and late apoptosis. The presence of CCF–HIONP improves both the rise in the proportion of cells with early and late

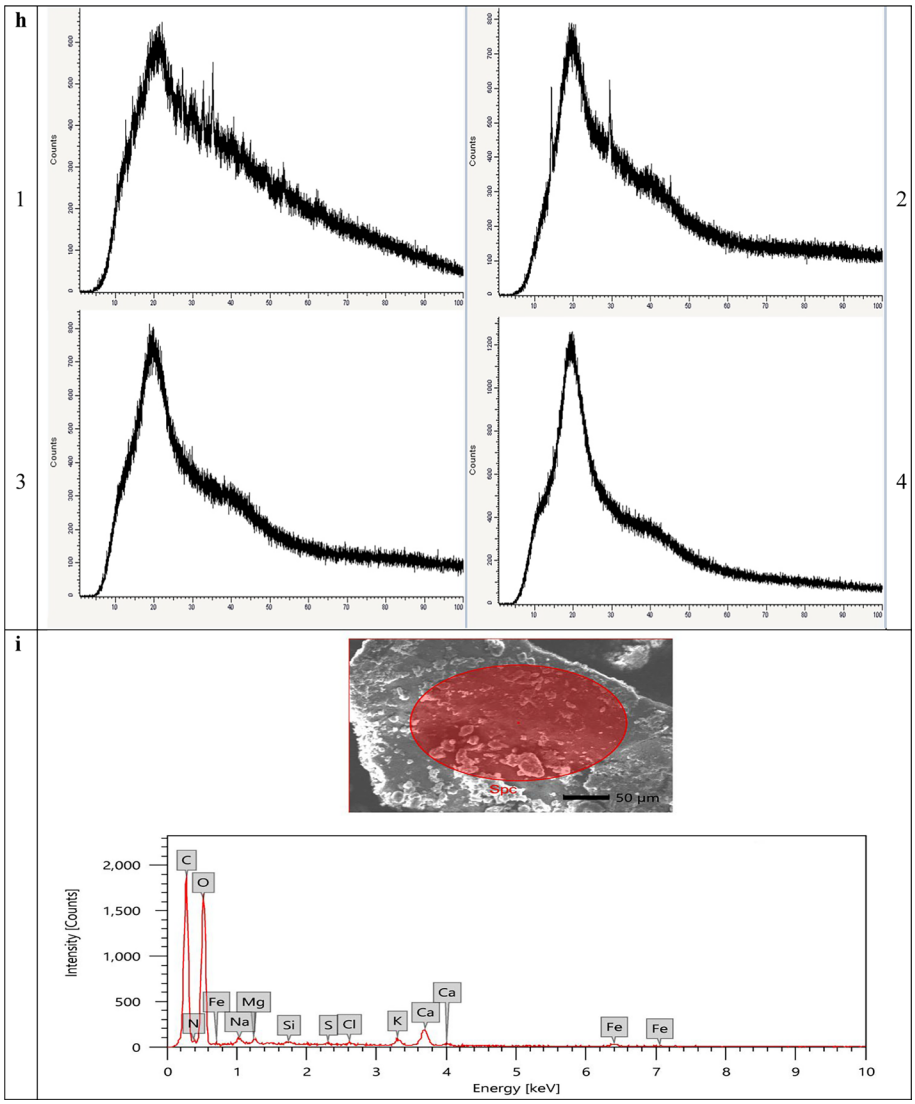

Fig. 2 continued

apoptosis in LCA A549 cells treated with laser (PDT) and high-frequency ultrasound (HIFU–SDT). The obtained data showed that HIFU–US is more effective than IRL at raising the proportion of LCA A549 cells with early and late apoptosis, both with and without the CCF–HIONP. For integration with laser, high-frequency ultrasound was chosen. The combination therapy approach (HIFU–SPDT) in the presence of CCF–HIONP is the most effective way to increase the proportion of LCA A549 cells with early and late apoptosis, as compared to using IRL or HIFU–US alone. Comparable observations were found for the proportion of necrotic cells in LCA A549 cells treated with either CCF–HIONP without activation or with lasers and high-frequency ultrasound without CCF–HIONP. The inclusion of CCF–HIONP improves both the elevation in the proportion of necrotic cells in LCA A549 cells treated with high-frequency ultrasound (HIFU–SDT) and laser (PDT). The obtained data showed that HIFU–US is more effective than IRL at increasing the proportion of necrotic

LCA A549 cells, both with and without the CCF–HIONP. The combined therapy strategy (HIFU–SPDT) in the presence of CCF–HIONP is most successful in elevating the percentage of LCA A549 cells with necrosis as compared to using IRL or HIFU–US alone Fig. 3c.

Autophagy cell death mechanism of PDT, HIFU–SDT and HIFU–SPDT in presence and absence of (CCF–HIONP) upon treatment of LCA A549

The SRB assay and microscopic examination indicate that program cell death other than apoptosis by autophagy in response to CCF–HIONP may be the cause of the decrease in cell viability. In order to investigate the process of cell death (autophagy), LCA A549 cells were subjected to different activation modalities for a duration of 24 h, both in the presence and absence of CCF–HIONP. When AO, a fluorophore that accumulates in acidic vesicular organelles (AVO) like autolysosomes at high concentrations, dimerizes and causes a green metachromatic shift to red, which can be assessed to study autophagy, the treated cells showed an increase in red intensity and a decrease in green intensity. LCA A549 cells treated with either CCF–HIONP without activation or with lasers and high-frequency ultrasound without CCF–HIONP showed a substantial increase in the percentage of cells undergoing autophagy. The presence of CCF–HIONP increases the percentage of autophagous cells in LCA A549 cells treated with both high-frequency ultrasound (HF–SDT) and laser photodynamic therapy (PDT). The obtained data showed that HIFU–US is more effective than IRL at raising the percentage of LCA A549 cells undergoing autophagy, both with and without the CCF–HIONP. For integration with laser, high-frequency ultrasound

(See figure on next page.)

Fig. 3 **a** The effect of different treatment modalities on lung cancer (A549) cell viability; a. microscopic investigations and b. dose response curve in all in vitro study groups; cell viability (%): F = 5.996 $p < 0.001$*. [a]: Significant with A549 untreated group, [b]: Significant with CCF@HIONP treated only group, [c]: Significant with laser only group, [d]: Significant with high-frequency ultrasound only group, [e]: Significant with laser + high-frequency ultrasound only group. **b** The effect of different treatment modalities on lung cancer (A549) cell cycle distribution in all in vitro study groups; SubG1(%):F(P): F = 158.397E3 $p < 0.001$*, G0/G1(%): F = 27.168 p < 0.001*, S(%): F = 56.195 $p < 0.001$*, G2/M(%): F = 36.376 $p < 0.001$*. [a]: Significant with A549 untreated group, [b]: Significant with CCF@HIONP treated only group, [c]: Significant with laser only group, [d]: Significant with high-frequency ultrasound only group, [e]: Significant with laser + high-frequency ultrasound only group. **c** The effect of different treatment modalities on lung cancer (A549) apoptosis and necrosis in all in vitro study groups; early apoptosis (%): F = 42.702 $p < 0.001$*, late apoptosis (%): F = 278.757 $p < 0.001$*, early and late apoptosis (%): F = 259.834 $p < 0.001$*, necrosis (%): F = 34.113 $p < 0.001$*, total cell death (%): F = 1.297E3 $p < 0.001$*.[a]: Significant with A549 untreated group, [b]: Significant with CCF@HIONP treated only group, [c]: Significant with laser only group, [d]: Significant with high-frequency ultrasound only group, [e]: Significant with laser + high-frequency ultrasound only group. **d** The effect of different treatment modalities on lung cancer (A549) autophagy in all in vitro study groups; autophagy (%): F = 97.107 $p < 0.001$*. [a]: Significant with A549 untreated group, [b]: Significant with CCF@HIONP treated only group, [c]: Significant with laser only group, [d]: Significant with high-frequency ultrasound only group, [e]: Significant with laser + high-frequency ultrasound only group. **e** The effect of different treatment modalities on lung cancer (A549) migration; 1. A549 untreated, 2. A549 treated with laser + high-frequency ultrasound only, 3. A549 treated with CCF@HIONP + laser + high-frequency ultrasound. wound clousure-24h (%): F = 2.329E3 $p < 0.001$*, wound clousure-48h (%): F = 830.700 $p < 0.001$*, wound clousure-24h (%): F = 798.931 $p < 0.001$*. [a]: Significant with A549 untreated group, [b]: Significant with CCF@HIONP treated only group, [c]: Significant with laser only group, [d]: Significant with high-frequency ultrasound only group, [e]: Significant with laser + high-frequency ultrasound only group

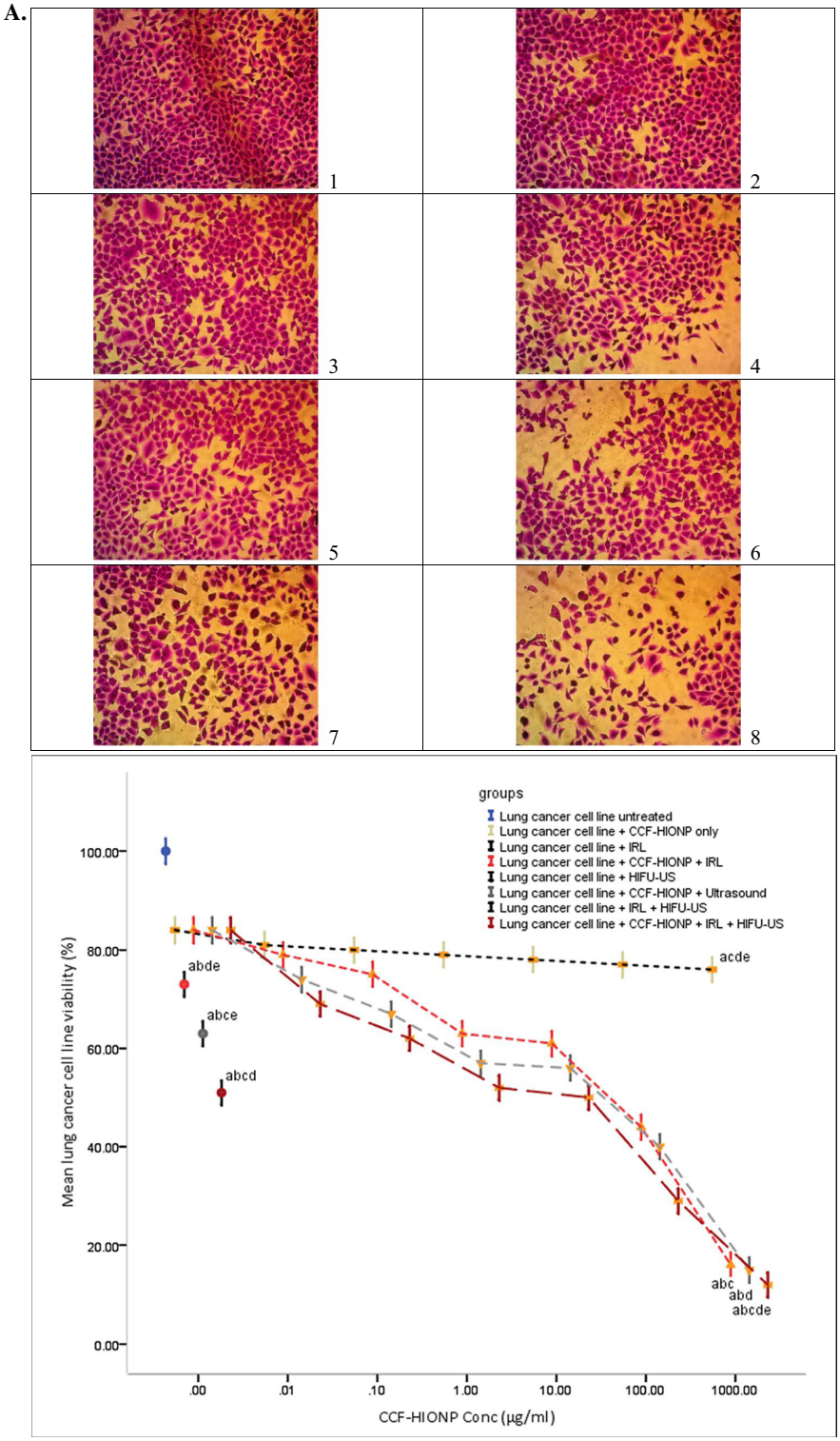

Fig. 3 (See legend on previous page.)

was chosen. The combined therapy strategy (HIFU–SPDT) in the presence of CCF–HIONP is most successful in elevating the percentage of LCA A549 cells undergoing autophagy as compared to using IRL or HIFU–US alone Fig. 3d.

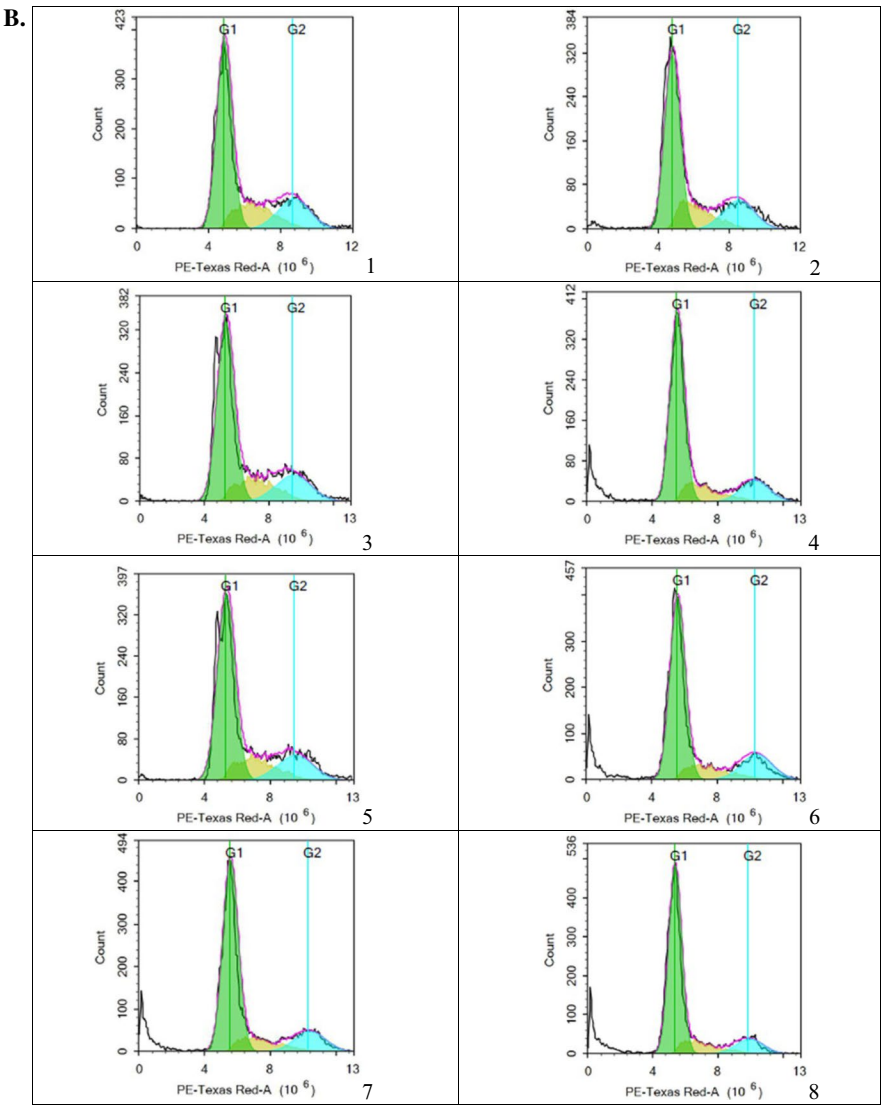

Fig. 3 continued

Cell migration inhibition mechanism of PDT, HIFU–SDT and HIFU–SPDT in presence and absence of (CCF–HIONP) upon treatment of LCA A549

The cell migration inhibitory effect as a result of different activation modalities with and without CCF–HIONP was investigated in LCA A549 cells after 24 h treatments, and wound closure until the closure of control untreated cells 72 h was assessed daily using the scratch assay. The treatment of the LCA A549 cell line with the combination therapy approach (HIFU–SPDT) in presence of CCF–HIONP demonstrated a notable decline in LCA A549 cell migration with respect to untreated control group, illustrating the potential anti-migratory effect Fig. 3e.

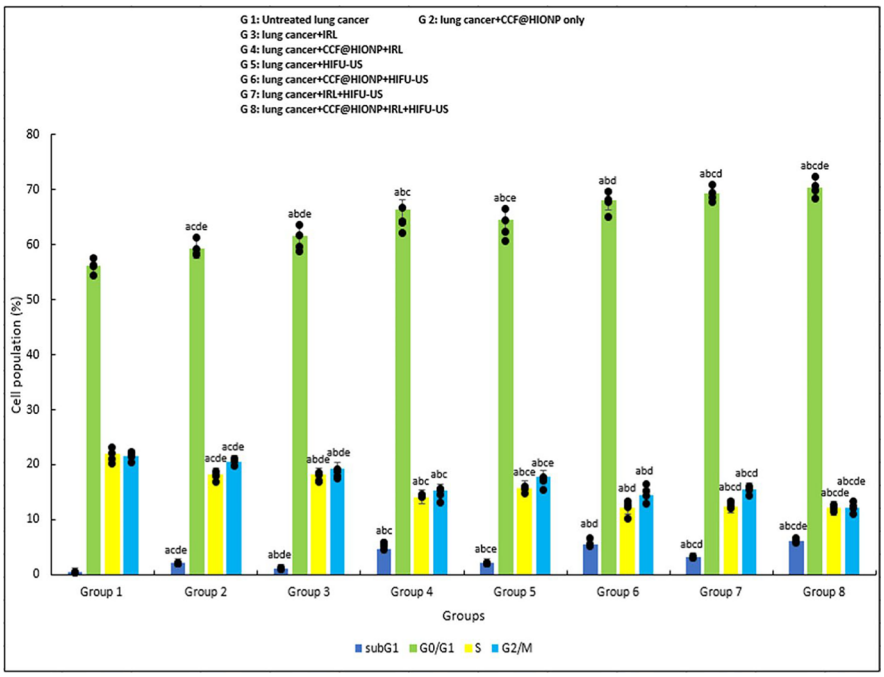

Fig. 3 continued

(CCF–HIONP) PDT, HIFU–SDT, HIFU–SPDT and oxidative stress in vivo LCA models

Figure 4a displays the effects of CCF–HIONP; PDT, HIFU–SDT, and HIFU–SPDT on lipid peroxidation oxidative stress MDA parameter in each of the experimental groups' mice. When comparing the untreated benzo[a]pyrene LCA-induced control mouse group to the non-irradiated group of mice treated with CCF–HIONP alone, the MDA showed very modest alterations in the sera. The untreated benzo[a] pyrene LCA-induced control animals had significantly greater values of this parameter compared to the control normal healthy mice. Furthermore, all benzo[a]pyrene LCA-induced mice treated with laser, high-frequency ultrasound, or combination of laser and high-frequency ultrasound alone groups exhibited a substantial rise in concentrations of MDA relative to the control normal mice. In contrast to the benzo[a] pyrene LCA-induced control animals, MDA levels were much lower in the laser, high-frequency ultrasound, and combination of laser and high-frequency ultrasound activated groups when CCF–HIONP was given, but this effect did not reach the level of control normal mice.

(CCF–HIONP) PDT, HIFU–SDT, HIFU–SPDT and the antioxidant system in vivo LCA models

Figure 4a illustrates how CCF–HIONP, PDT, HIFU–SDT, and HIFU–SPDT affected the antioxidant indicators (Catalase, SOD, TAC, GR, GPx and GST) in each of the research groups of mice. The benzo[a]pyrene LCA-induced control group was compared to the CCF–HIONP alone without activation. Only marginally significant alterations were seen in the TAC level, GST, GPx, GR, SOD, and catalase activities. The untreated control benzo[a] pyrene LCA-induced mice exhibited considerably lower levels of Catalase, SOD, GR, GPx and GST and TAC than the normal control mice. Furthermore, with respect to the healthy

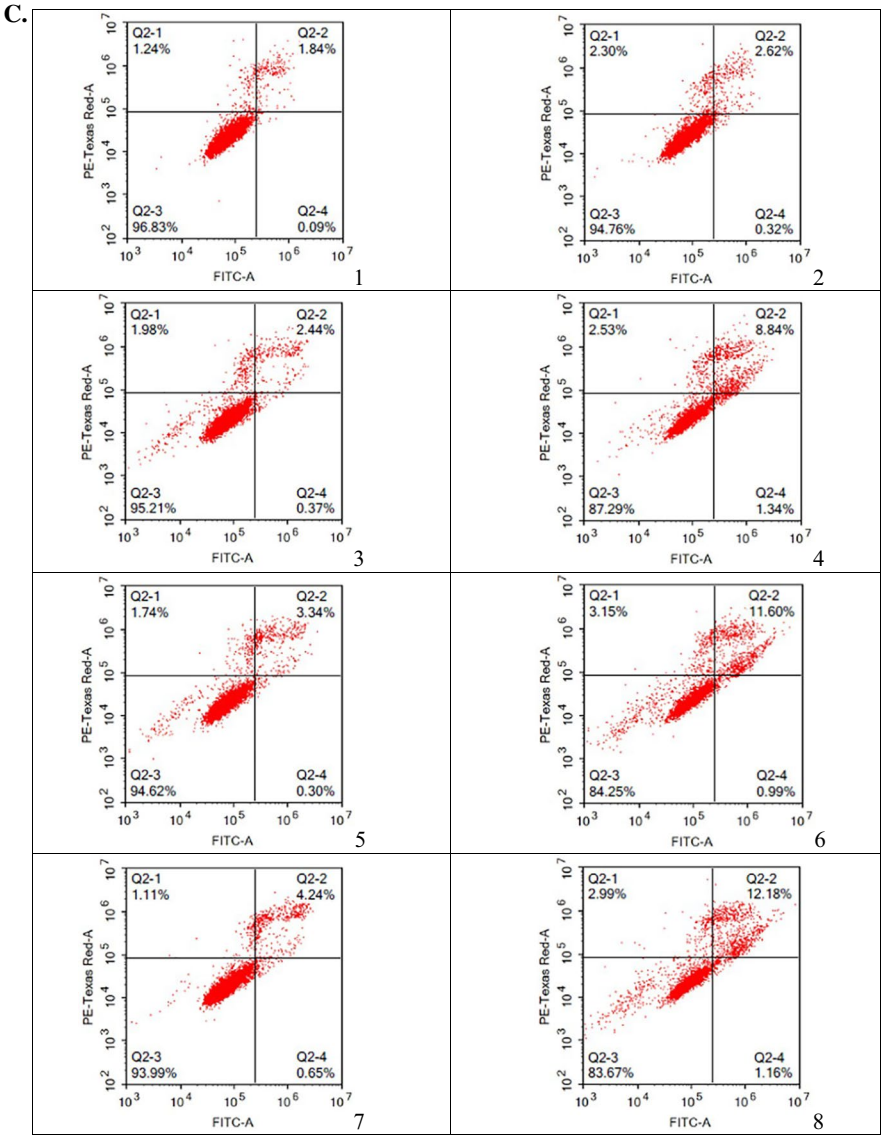

Fig. 3 continued

control group of mice, all benzo[a]pyrene LCA-induced mouse groups treated with laser, high-frequency ultrasound, or combination of laser and high-frequency ultrasound solely exhibited a significant reduction in levels as well as Catalase, SOD, TAC, GR, GPx and GST activities. CCF–HIONP in the laser, high-frequency ultrasound, and combination of laser and high-frequency ultrasound activated groups showed a considerable elevation in the TAC level and the Catalase, SOD, GR, GPx and GST activities, but did not approach the level of control normal group levels, in contrast to the untreated benzo[a]pyrene LCA-induced control mice.

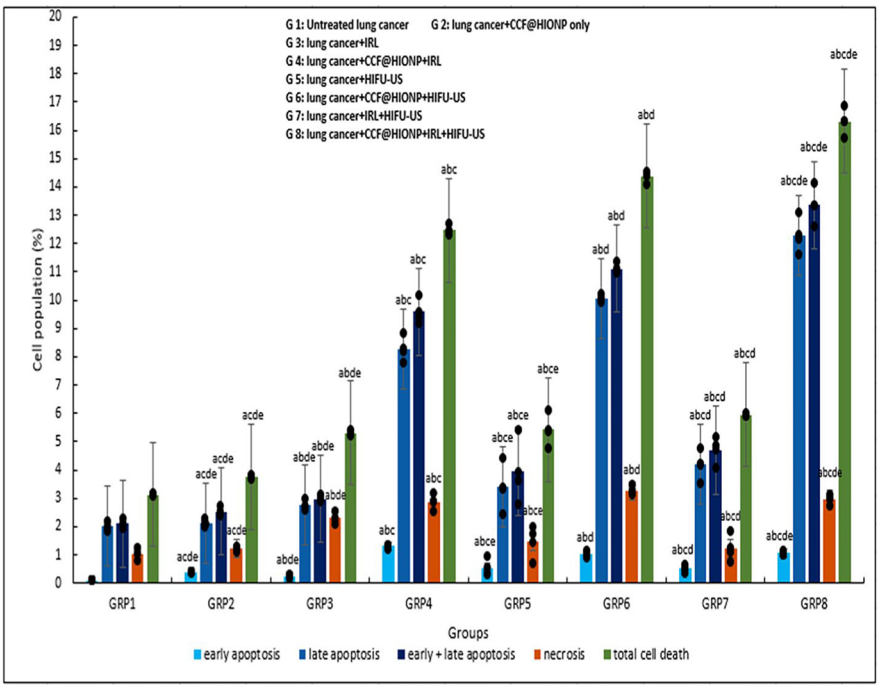

Fig. 3 continued

(CCF–HIONP) PDT, HIFU–SDT, HIFU–SPDT treatment improved liver functions in vivo LCA models

Figure 4b shows the results of the function liver tests performed on each group under study. While the levels in the sera of the untreated control benzo[a]pyrene LCA-induced group were higher significantly than those in the control normal healthy mice, the AST and ALT levels in the mice treated with CCF–HIONP alone without irradiation showed only marginally different changes from the untreated benzo[a]pyrene LCA-induced control group. Furthermore, all benzo[a]pyrene LCA-induced mice treated with laser, high-frequency ultrasound, or combination of laser and high-frequency ultrasound alone groups displayed a significantly higher level of AST and ALT in comparison to the control normal group. Furthermore, as comparison to the untreated benzo[a]pyrene LCA-induced control mice, the level of AST and ALT was dramatically reduced when CCF–HIONP was given to the laser, high-frequency ultrasound, and combination of laser and high-frequency ultrasound activated groups; nevertheless, the normal control group levels was not reached.

(CCF–HIONP) PDT, HIFU–SDT, HIFU–SPDT treatment improved kidney functions in vivo LCA models

Figure 4b shows the results of the function kidney tests performed all the groups under study. When compared to the untreated control benzo[a]pyrene LCA-induced mice, the serum levels of creatinine or urea in mice treated with CCF–HIONP alone without irradiation showed only marginally significant changes; however, this

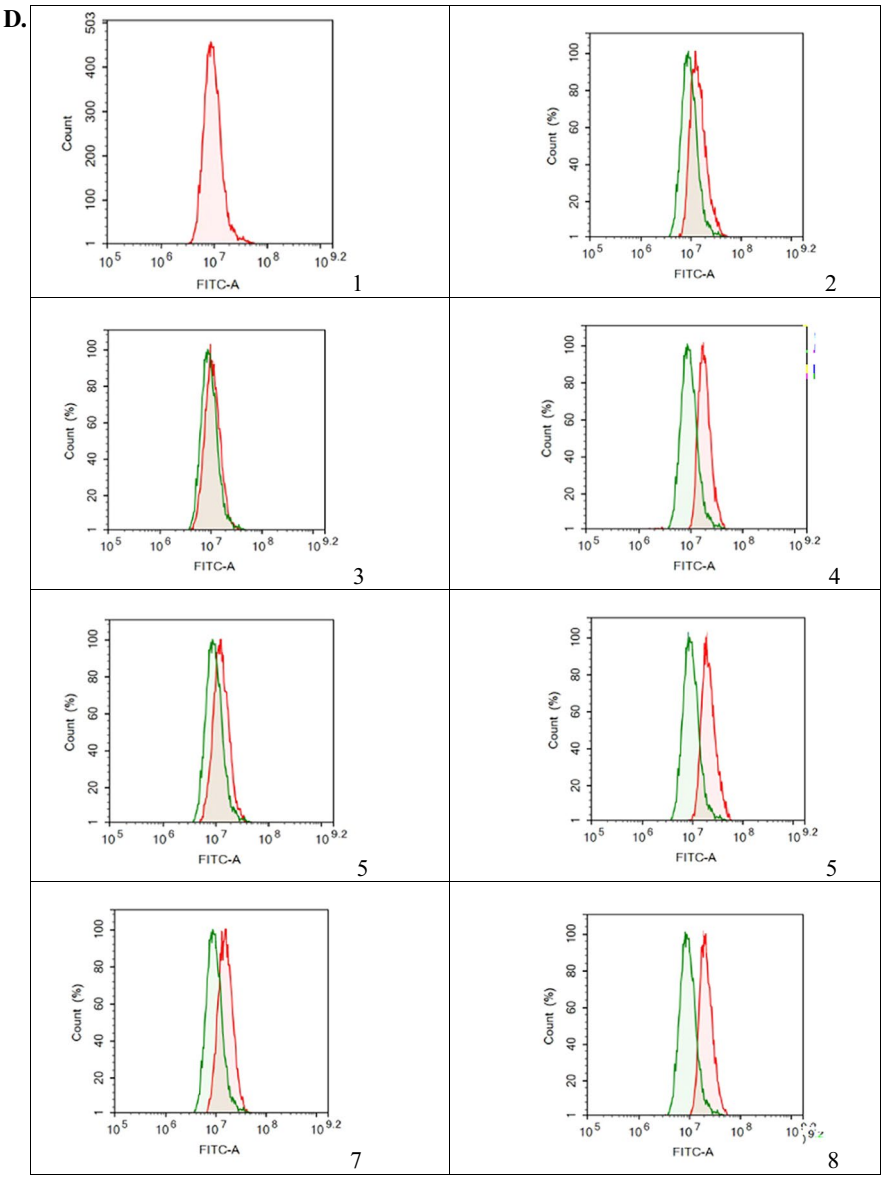

Fig. 3 continued

parameter levels in the untreated control benzo[a]pyrene LCA-induced mice were higher significantly when compared to the control normal healthy mice. Furthermore, all benzo[a]pyrene LCA-induced mice treated with laser, high-frequency ultrasound, or combination of laser and high-frequency ultrasound alone groups showed a statistically significant elevation in creatinine and urea levels relative to the control normal group. Furthermore, when compared to the untreated control benzo[a]pyrene LCA-induced mice, the administration of CCF–HIONP in the laser, high-frequency ultrasound, and combination of laser and high-frequency ultrasound activated groups considerably reduced the levels of creatinine and urea; however, these levels did not reach the control normal group.

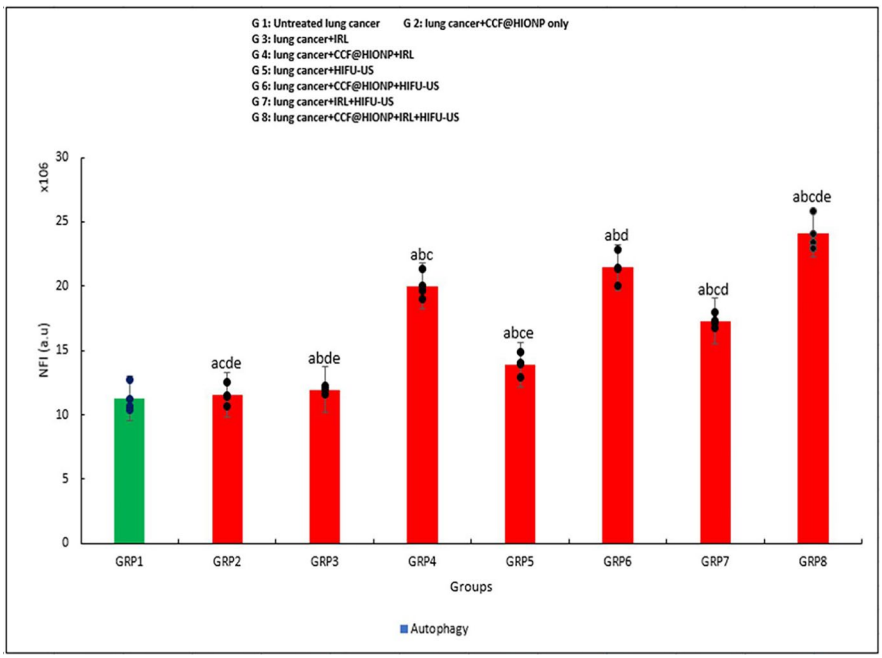

Fig. 3 continued

(CCF–HIONP) PDT, HIFU–SDT, HIFU–SPDT anticancer, antiproliferative and antiangiogenic effects in vivo LCA models

Figure 4c shows the effects of CCF–HIONP on the genes relative expressions of VEGF, TNF alpha, Bcl-2, Bax, Caspase (3, 9), and p53 in all groups under study. When CCF–HIONP was administered to mice in isolation without activation, the expression of VEGF, TNF alpha, Bcl-2, Bax, Caspase (3, 9), and p53 changed only slightly in comparison to the untreated control benzo[a]pyrene LCA-induced group. In contrast, the untreated control benzo[a]pyrene LCA-induced group's levels of caspase (3, 9), p53, TNF alpha, and Bax were lower significantly, while those of Bcl-2, and VEGF were higher significantly than those of control normal, healthy mice. Furthermore, in comparison to the control group of healthy mice, all benzo[a]pyrene LCA-induced mice treated with laser, high-frequency ultrasound, or a combination of laser and high-frequency ultrasound alone groups exhibited significantly elevated levels of VEGF and Bcl-2 gene expressions and decreased significantly levels of caspase (3, 9), p53, TNF alpha, and Bax gene expressions. The delivery of CCF-HIONP to the laser, high-frequency ultrasound, and combination of laser and high-frequency ultrasound activated groups resulted in significant increases in the expressions of the genes caspase (3, 9), p53, TNF alpha, and Bax and significant decreases in the expressions of the genes VEGF and Bcl-2, as compared to the control untreated benzo[a]pyrene LCA-induced group.

(CCF–HIONP) PDT, HIFU–SDT, HIFU–SPDT histopathological effect on in vivo LCA models

Figure 4d displays the H&E stained tissue sections from all mouse study groups that demonstrate how CCF–HIONP, PDT, HIFU–SDT, and HIFU–SPDT affect LCA caused by benzo[a]pyrene. According to the histological study, all of the tumors in

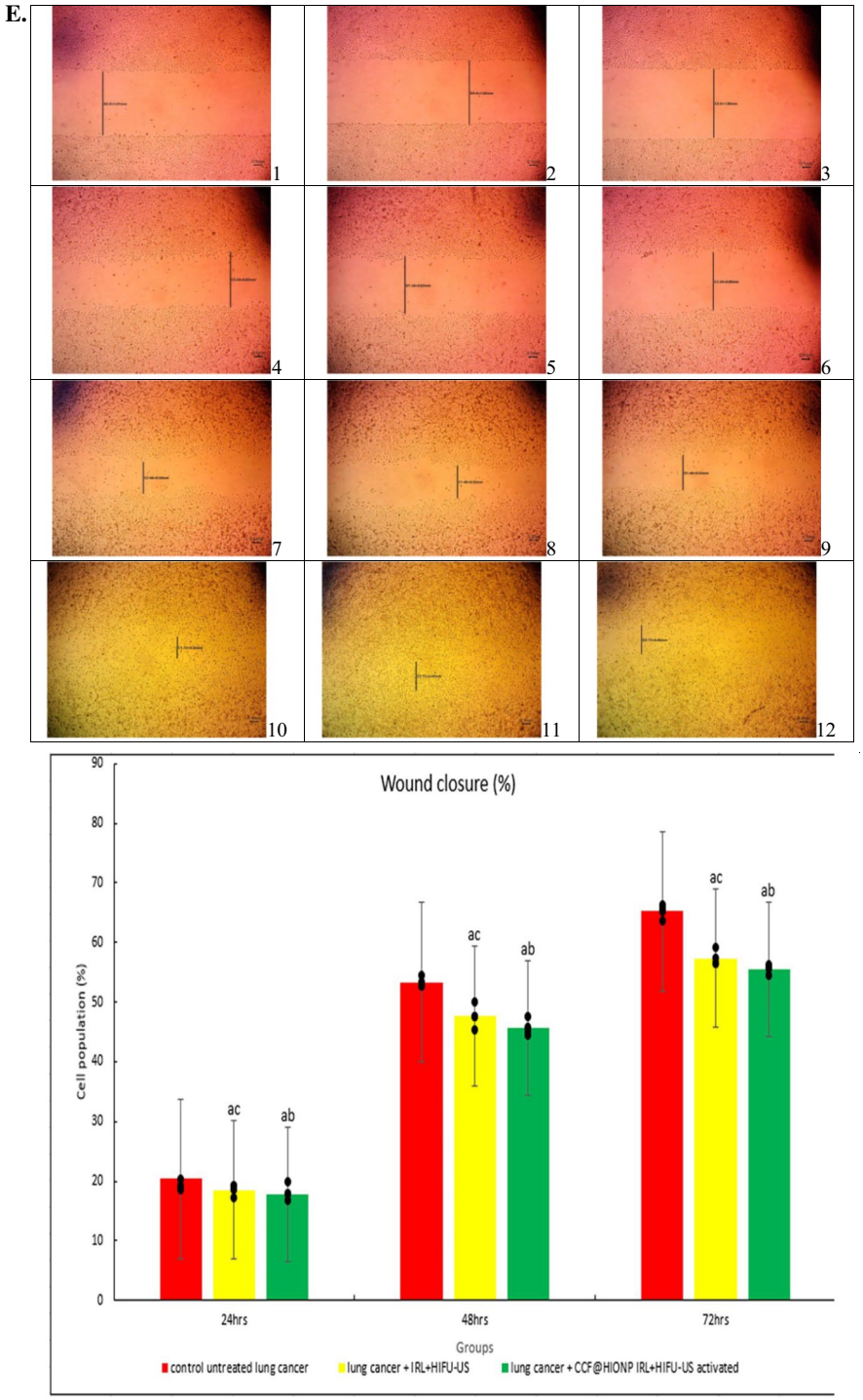

Fig. 3 continued

the untreated control benzo[a]pyrene LCA-induced group exhibited 5% necrosis and were completely composed of extremely malignant cells. In comparison to the untreated control benzo[a]pyrene LCA-induced mice, the histologically induced LCA tissues showed only marginally significant alterations in the mice treated with

CCF–HIONP alone, without irradiation. The administration of CCF–HIONP in the laser, high-frequency ultrasound, and combination of laser and high-frequency ultrasound activated groups' manifested significantly necrotic large foci areas (85–90%) in regards to the untreated control benzo[a]pyrene LCA-induced mice. In addition, all benzo[a]pyrene LCA-induced mice treated with laser, high-frequency ultrasound, or combination of laser and high-frequency ultrasound only demonstrated considerable necrosis areas with respect to the untreated control benzo[a]pyrene LCA-induced group.

Discussion

The clinical management of LCA remains a difficulty despite the numerous advancements in the fields of oncological diagnostics and medicinal sciences. Delays in diagnosis, metastatic tendency, multidrug resistance, and an unpredictable tumor environment are some of the main aspects that add to the unsolved mystery of LCA and eventually create obstacles for treatment approaches. Researchers' attention has been heavily focused in the last few years on creating novel compounds and medication delivery methods that would increase efficacy while lowering toxicity. Plant-based nanoparticle therapies are currently being investigated because of their high availability, low cost, and little potential negative effects (Carrasco-Esteban et al. 2021; Abd El-Kareem 2019; Soundararajan and Kim 2018; Navada et al. 2022).

The results of SRB assay is a valuable test that measures viable cell count precisely and evaluates the cytotoxicity of drugs used in cancer treatment. In addition, one of the most vital mechanisms causing cancer is the disruption of the cell cycle, which is the basic

(See figure on next page.)

Fig. 4 **a** The effect of different treatment modalities on antioxidants activities, capacities and MDA in all study groups; 1. GSH (mg/dl): F(P): F = 369.255 $p < 0.001$*, 2. GR (mU/ml): F = 332.999 $p < 0.001$*, 3. GST (U/ml): F = 716.937 p < 0.001*, 4. GPx (mU/ml): F = 1.534E4 p < 0.001*, 5. SOD (U/ml): F = 3.905E6 $p < 0.001$*, 6. CAT (mU/ml): F = 1.733E5 $p < 0.001$*, 7. TAC (mM/L): F = 365.105 $p < 0.001$*, 8. MDA (nmol/ml): F = 9.878E4 $p < 0.001$*. [a]: Significant with normal group, [b]: Significant with lung cancer untreated group, [c]: Significant with CCF@HIONP treated only group, [d]: Significant with laser only group, [e]: Significant with high-frequency ultrasound only group, [f]: Significant with laser + high-frequency ultrasound only group. **b** The effect of different treatment modalities on renal and hepatic biomarkers in all study groups; F: value for ANOVA test 1. ALT (U/l): F = 9.568E3 p < 0.001*, 2. AST (U/l): F = 1.861E5 $p < 0.001$*, 3. Urea (mg/dl): F = 4.549 E3 $p < 0.001$*, 4. Creatinine (mg/dl): F = 531.321 $p < 0.001$*. [a]: Significant with normal group, [b]: Significant with lung cancer untreated group, [c]: Significant with CCF@HIONP treated only group, [d]: Significant with laser only group, [e]: Significant with high-frequency ultrasound only group, [f]: Significant with laser + high-frequency ultrasound only group. **c** The effect of different treatment modalities on p53, Bax, Caspase (9,3), TNF alpha, VEGF, Bcl-2 qRT-PCR relative genes expressions in all study groups; F: value for ANOVA test. p53 F = 693.721 $p < 0.001$*, Bax F = 1.191E3 $p < 0.001$*, Caspase 9 F = 1.090E3 $p < 0.001$*, Caspase 3 F = 899.872 $p < 0.001$*, TNFalpha F = 400.998 $p < 0.001$*, VEGF F = 199.784 $p < 0.001$*, Bcl-2 F = 237.176 $p < 0.001$*. [a]: Significant with normal group, [b]: Significant with lung cancer untreated group, [c]: Significant with CCF@HIONP treated only group, [d]: Significant with laser only group, [e]: Significant with high-frequency ultrasound only group, [f]: Significant with laser + high-frequency ultrasound only group. **d** The H&E lung tissue stained section demonstrating the effect of different treatment modalities on cellular level in all study groups; 1. normal untreated group, 2. benzo[a]pyrene induced LCA group without any treatment, 3. CCF@HIONP treated group without activation, 4. benzo[a]pyrene induced LCA group treated with laser only, 5. benzo[a]pyrene induced LCA group treated with laser in presence of CCF@HIONP, 6. benzo[a]pyrene induced LCA group treated with high-frequency ultrasound only, 7. benzo[a]pyrene induced LCA group treated with high-frequency ultrasound in presence of CCF@HIONP, 8. benzo[a]pyrene induced LCA group treated with combined modalities laser/high-frequency ultrasound only, 9. benzo[a]pyrene induced LCA group treated with combined modalities laser/high-frequency ultrasound in presence of CCF@HIONP

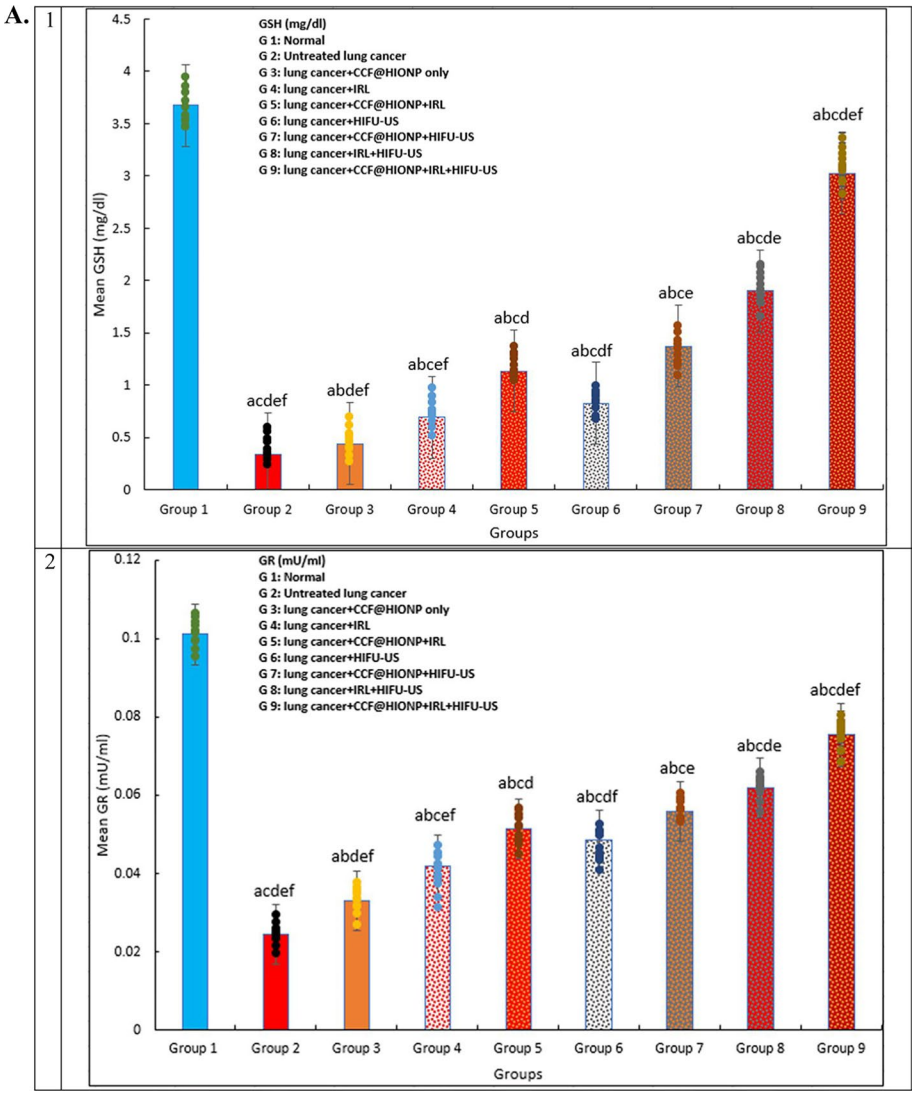

Fig. 4 (See legend on previous page.)

process that governs a cell's life activities. Moreover, three forms of programmed cell death that counteract biological processes of proliferation and are essential to appropriate development are apoptosis, necrosis, and autophagy. Since most malignancies require tumor cells to have the ability to overpower apoptosis in order to survive, it is thought that the formation and growth of tumors are related to blocked apoptosis and aberrant proliferation (Kim et al. 2012; Tonder et al. 2015; Noguchi et al. 2020; Wang and Kanneganti 2021).

The findings of the SRB assay (cytotoxicity) and flow cytometry (cell cycle analysis, apoptosis, necrosis, and autophagy) in this study showed that there was only a minor impact on the LCA–A549 cell line following a 24-h incubation period and treatment with CCF–HIONP without activation. The LCA–A549 cell line is not significantly affected by the use of laser and high-frequency ultrasound in the absence of CCF–HIONP. The efficacy of the high-frequency ultrasound (HIFU–SDT) and the laser

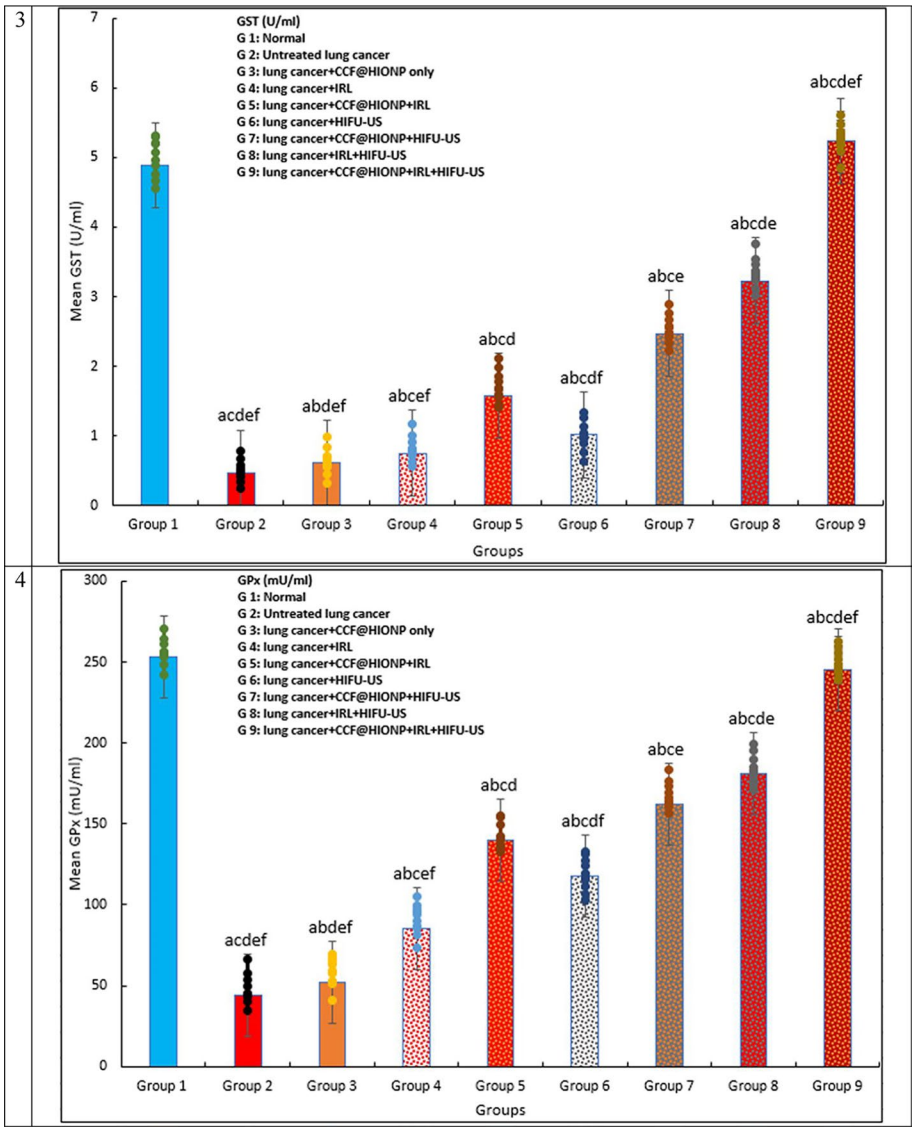

Fig. 4 continued

(PDT) is increased when CCF–HIONP is present. The obtained results demonstrated that the combined therapeutic method (HIFU–SPDT) is more effective than either red laser or high-frequency ultrasound alone in treating the LCA–A549 cell line (cell viability decreased in a dose-responsive manner, the cell cycle progression in G0/G1 was slowed down, and cell death was induced as evidenced by an elevation in the population of Pre-G cells, an increase in early and late apoptosis and necrosis, and an elevation in autophagic cell death). Our findings are consistent with prior research (Buckner et al. 2019; Shaer and Al-Abbas 2022; Ibrahim et al. 2023).

A useful tool for studying the process of chemical carcinogenesis caused by polycyclic aromatic hydrocarbons (PAHs) is the lung tumor-genesis system in mice. Benzo[a] pyrene is the most thoroughly studied PAH, it is pervasive in the environment and it is a particularly potent carcinogen. The WHO further reported that benzo[a]pyrene is

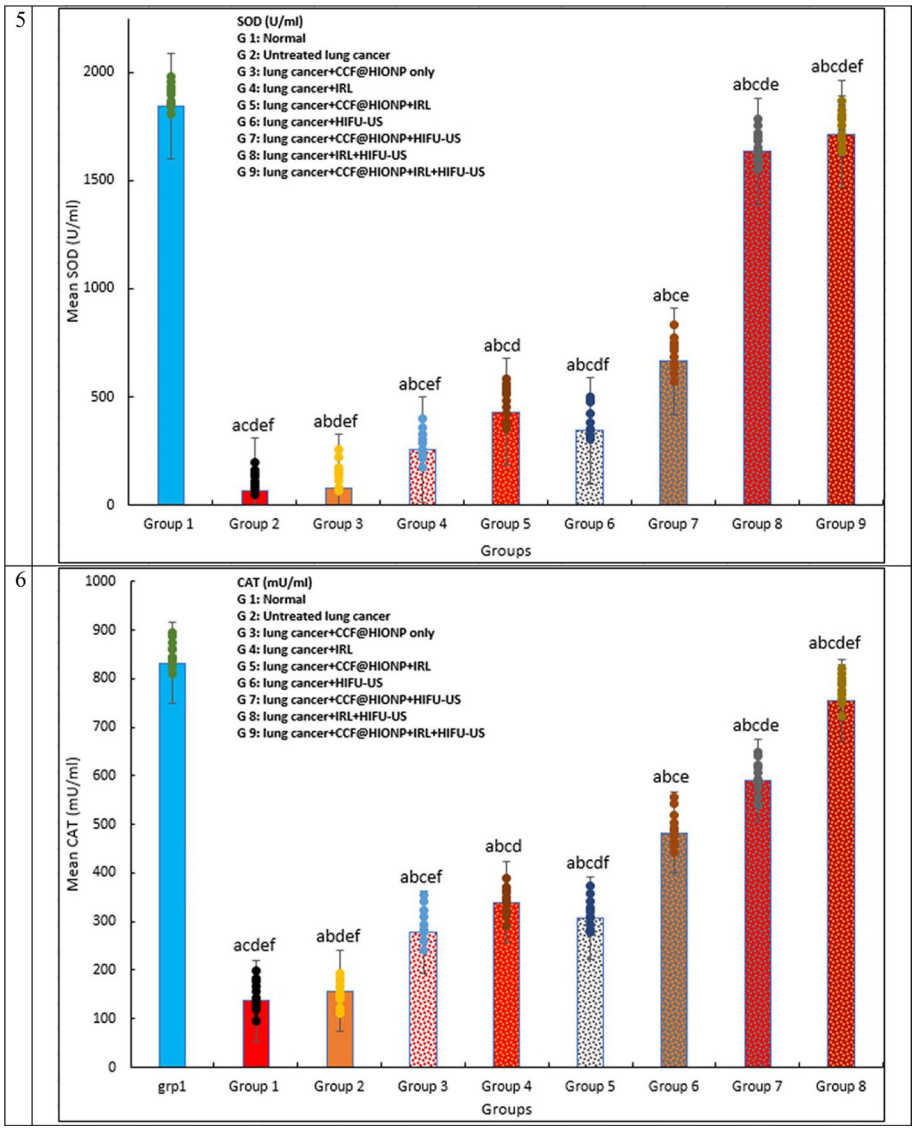

Fig. 4 continued

usually chosen as the benchmark by which other PAHs' cancer-causing potential is evaluated. Furthermore, benzo[a]pyrene is known to cause lung cancer in humans, and both the compound itself and ambient mixes containing benzo[a]pyrene have been shown to cause cancer in a variety of rodent species. It is well known that benzo[a]pyrene generates large numbers of extremely reactive, poisonous, and mutagenic free radicals as well as non-radical oxidizing species. The process of tissue lipid peroxidation is mediated by these harmful radicals. The sensitive aspect of malignant circumstances is lipid peroxidation-induced tissue damage, and any degradation or rupture of the membrane can cause these enzymes to leak out of the tissues. It has been found through experimental research that the carcinogenesis process is modifiable. Chemo-prevention/therapy through the administration of or ingestion of foods and drinks containing chemo-preventive/therapeutic substances is one of anti-cancer research method (Rajendran et al.

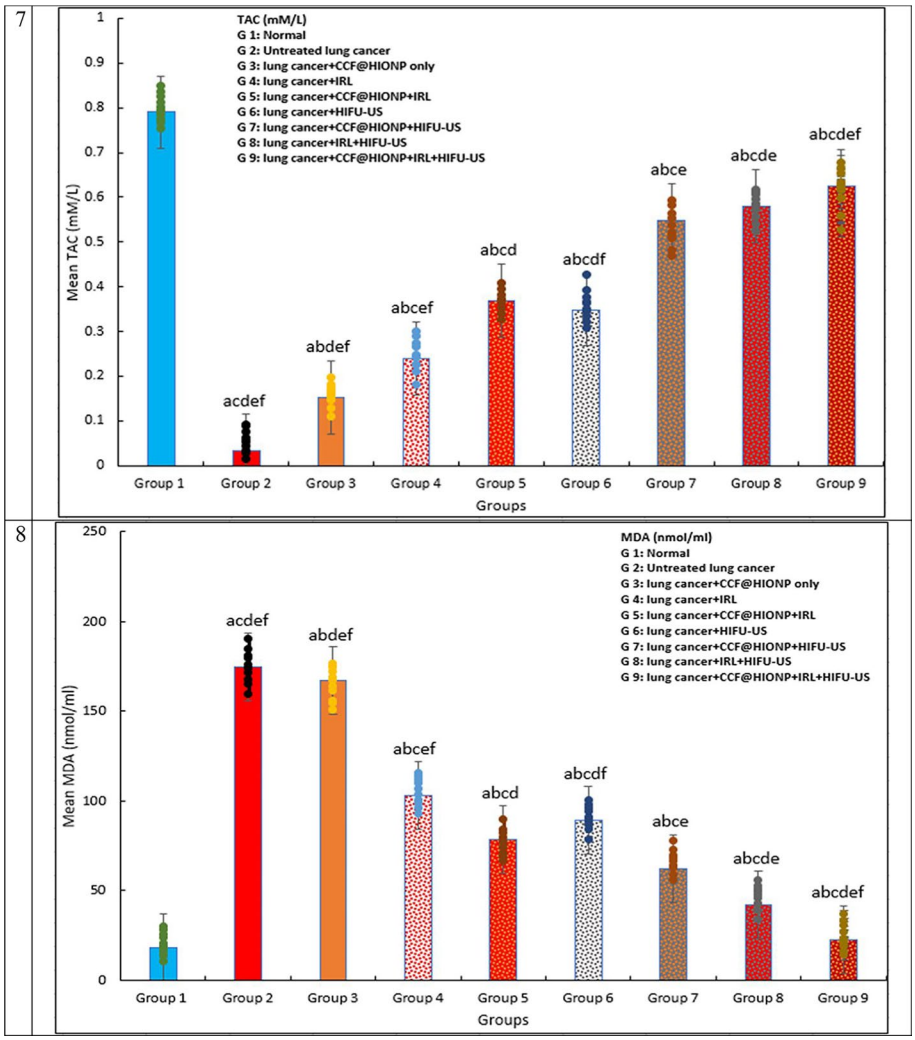

Fig. 4 continued

2008; Kamaraj et al. 2009; Omidian et al. 2017; Du et al. 2021; Shahid et al. 2023; Wu et al. 2023).

The current investigation offers proof of the oxidants that the benzo[a]pyrene induced LCA is advancing. The MDA levels in the untreated control benzo[a]pyrene LCA-induced mice were significantly higher. Compared to untreated control benzo[a]pyrene LCA-induced mice, MDA levels were considerably reduced in all CCF–HIONP treated groups (non-irradiated, laser-activated, shockwave-activated, and combination of laser and shockwave-activated mice). Significant reductions in the TAC backup and in the activities of Catalase, GST, GPx, GR, and SOD further disrupt the antioxidant system. The antioxidant levels in the benzo[a]pyrene LCA-induced control mice that were not treated were significantly lower. Antioxidant levels were considerably higher in all CCF–HIONP treated groups (laser-activated, shockwave-activated, and combination of laser and shockwave-activated) than in untreated control benzo[a]pyrene LCA-induced mice. Previous studies have shown that induction of benzo[a]pyrene LCA results in a significant rise in MDA and a decrease in TAC, GST, Catalase, GPx, GR, SOD, and activity.

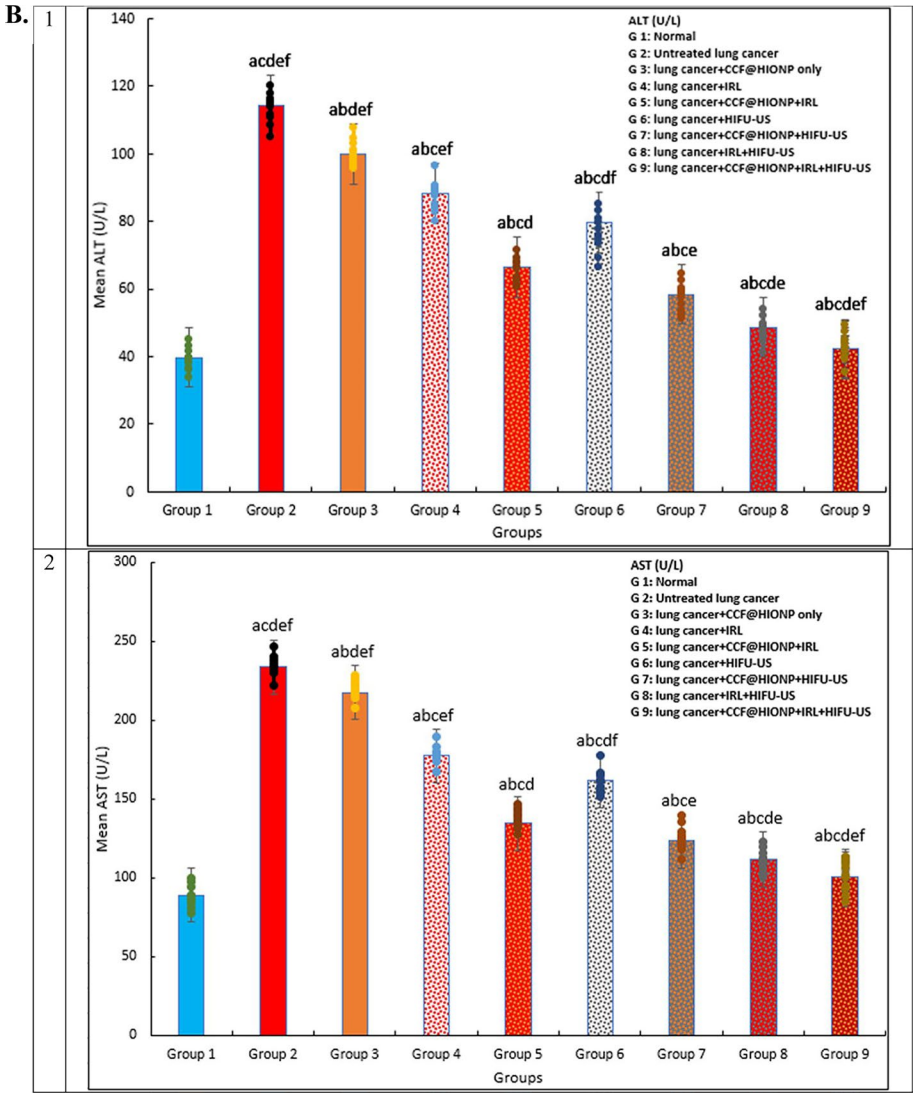

Fig. 4 continued

(Omidian et al. 2017; Du et al. 2021; Shahid et al. 2023; Dardeer et al. 2021a; Abd El-Kareem et al. 2023) It was discovered that mice with LCA generated by benzo[a]pyrene showed reduced activity in scavenging free radicals and were more vulnerable to lipid peroxidation than mice from healthy, normal control. As priory mentioned, benzo[a] pyrene LCA-induction promotes the generation of various free radical metabolites, leading to an excess and accumulation of ROS as well as an increase in the oxidation of cell phospholipid polyunsaturated fatty acid bilayers, which in turn raises MDA levels. The deterioration of enzymatic and non-enzymatic antioxidants is a critical step in the oxidative stress development and cancer evolve. These antioxidants, both enzymatic and non-enzymatic, were continuously depleted, which explained why they were needed to detoxify benzo[a]pyrene LCA-induced ROS and their metabolites, which explained why they were lacking. The accumulation of ROS may compromise the catalytic activity of enzymatic antioxidants. (Omidian et al. 2017; Du et al. 2021; Shahid et al. 2023; Deng

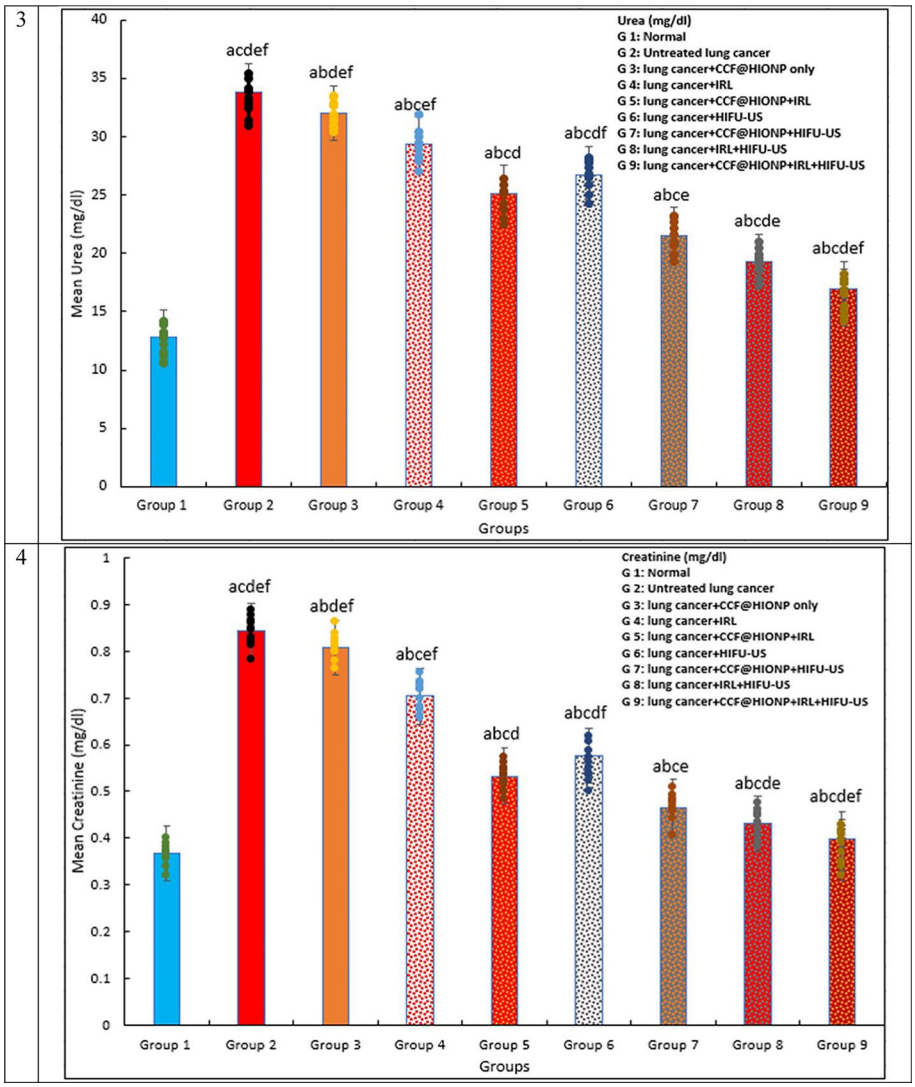

Fig. 4 continued

et al. 2018; Abd El-Kaream et al. 2019a, 2019b, 2019c; Jasim et al. 2019; Velli et al. 2019; Abdulrahman et al. 2020; Dardeer et al. 2021b; Nithya et al. 2023) Our findings demonstrated how the anti-lipid peroxidative action of non-activated part of CCF–HIONP is supported by its ability to generated free radical scavenge. Furthermore shows the effectiveness of CCF–HIONP action as HIFU–SPS and its activation by PDT, HIFU–SDT and HIFU–SPDT, which eliminated benzo[a]pyrene, the primary ROS source, causing a rise in antioxidant enzyme activities and a transition from a cancerous state to a state that is almost normal. Our results agreed with previous studies (Makawy et al. 2022; Selek et al. 2018; Silva and Alcorn 2019).

In the benzo[a]pyrene LCA-induced groups in our investigation, there was a substantial increase in ALT and AST, suggesting liver cell damage. Elevated levels of several liver enzymes in serum are associated with cellular leakage of those enzymes into the bloodstream, which is indicative of damage to the hepatocyte's integrity in the cell membrane

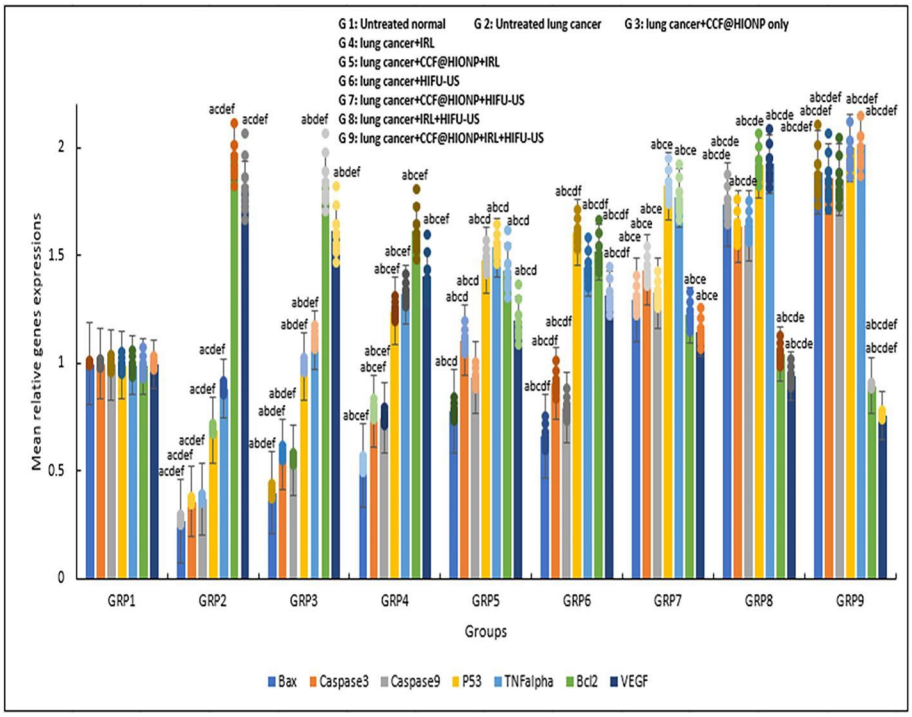

Fig. 4 continued

(Deng et al. 2018; Asha and Girija 2011; Kim et al. 2024; Sakthivel et al. 2019). Because benzo[a]pyrene disrupts metabolism and induces organ failure, this work results are in line with earlier studies in illustrating that hepatic function was reduced in benzo[a]pyrene LCA-induced animals as compared to normal control mice (Rajendran et al. 2008; Kamaraj et al. 2009; Omidian et al. 2017; Du et al. 2021; Jasim et al. 2019; Velli et al. 2019; Abdulrahman et al. 2020; Dardeer et al. 2021b; Nithya et al. 2023; Makawy et al. 2022; Selek et al. 2018; Silva and Alcorn 2019; Asha and Girija 2011; Kim et al. 2024). The current study discovered that CCF–HIONP decreased ALT and AST levels, indicating liver protection. Furthermore, this bolsters the protective efficacy of CCF–HIONP in averting hepato-dysfunction in mice induced by benzo[a]pyrene LCA. In addition, benzo[a]pyrene caused a clear elevation in urea and creatinine in the benzo[a]pyrene LCA-induced groups in this study, indicating renal damage. It has been demonstrated that cardiac and hepatic damage causes renal dysfunction in benzo[a]pyrene LCA-induced rats, resulting in increased tubular and glomerular congestion. Due to this congestion, results in an elevation in interstitial renal pressure over the entire capillary and tubule system. The findings of this investigation support previous findings by showing that, compared to control normal mice, benzo[a]pyrene LCA-induced mice had decreased renal function (Rajendran et al. 2008; Kamaraj et al. 2009; Omidian et al. 2017; Du et al. 2021; Abd El-Kaream et al. 2023; Deng et al. 2018; Jasim et al. 2019; Velli et al. 2019; Abdulrahman et al. 2020; Dardeer et al. 2021b; Nithya et al. 2023; Makawy et al. 2022; Selek et al. 2018; Silva and Alcorn 2019; Asha and Girija 2011; Kim et al. 2024; Sakthivel et al. 2019; Lei et al. 2023; Zhang et al. 2021). The current study discovered that CCF–HIONP decreased serum levels of creatinine and urea, which evoke kidney protection. Moreover, this validates

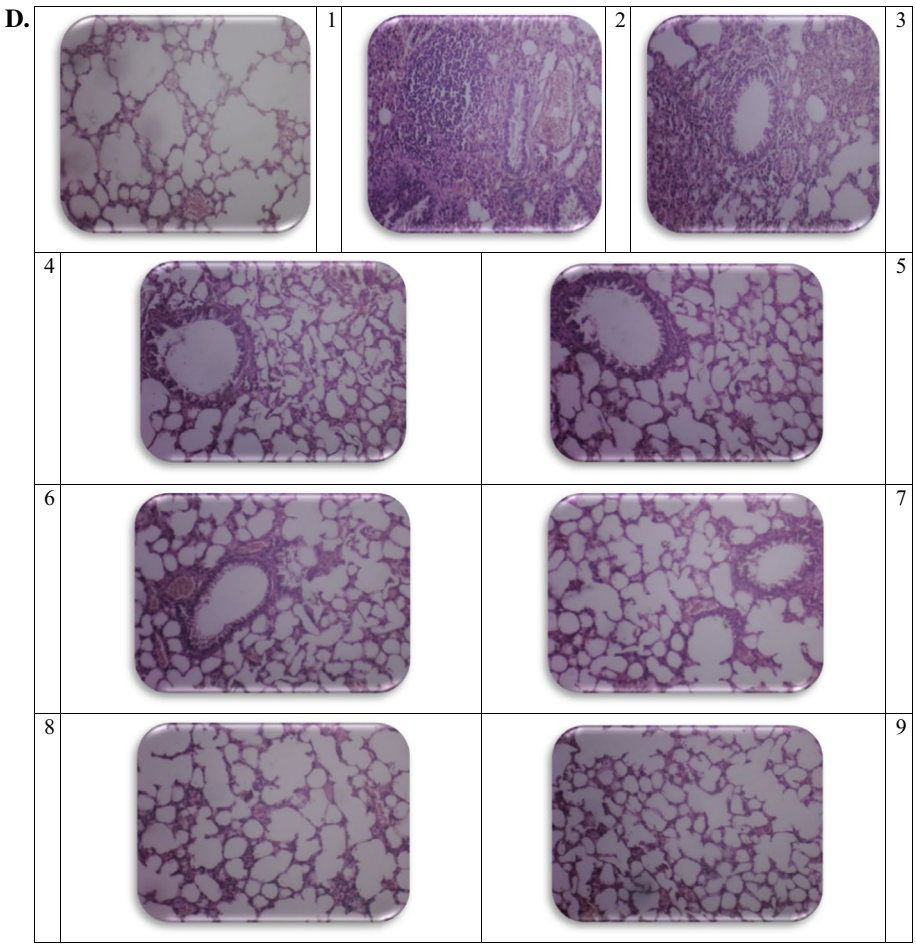

Fig. 4 continued

the preventative activity of CCF–HIONP in averting renal impairment in mice that is induced by benzo[a]pyrene LCA.

The expressions of Bax, Caspase (3,9), p53, TNF alpha, VEGF and Bcl-2 were molecularly assessed in the current study as indicators of benzo[a]pyrene-induced LCA treatment and inhibition of angiogenesis, respectively. The results indicate a significant negative correlation between the gene expressions and benzo[a]pyrene LCA-induction, but a positive marked correlation between the gene expressions and the presence of CCF–HIONP with different modalities treatment. The high-frequency ultrasound-photo-dynamic therapy with (CCF–HIONP) mice groups had significantly higher expression of the genes Bax, caspase 3, 9, p53, TNF alpha than did the PDT or HIFU–SDT with (CCF–HIONP), IRL or HIFU–US only without (CCF–HIONP), and the untreated benzo[a]pyrene LCA-induced mice. On the other hand, in the untreated benzo[a]pyrene LCA-induced animals, there was a positive association between VEGF and Bcl-2 expressions, whereas in the presence of CCF–HIONP, there was a negative marked correlation between VEGF and Bcl-2 expressions with treatment modalities. Compared to mice treated with PDT or HIFU–SDT with (CCF–HIONP) alone, and then IRL or HIFU–US alone without (CCF–HIONP) alone, the expressions of the VEGF

and Bcl-2 genes were considerably lower in mice treated with HIFU–SPDT therapy with (CCF–HIONP). In mice stimulated with benzo[a]pyrene LCA, expression was highest in the untreated group. Our study's results, which are consistent with those of other studies, show that expressions of Bax, Caspase (3,9), p53, TNF alpha, Bcl-2 and VEGF genes as a reliable indicators of cancer-relevant treatment (Abu Rakhey et al. 2022; Abd El-Kareem et al. 2023; Asha and Girija 2011; Sakthivel et al. 2019; Lei et al. 2023; Zhang et al. 2021; Han et al. 2020; Yang et al. 2024; Mueed et al. 2023; El Makawy et al. 2024).

As of right now, our findings suggest that CCF–HIONP may be used as a shockwave and photosensitizer to cure in vivo LCA induced by benzo[a]pyrene. The CCF–HIONP significantly inhibits tumor growth and induces cell death that could be triggered by activation chemical processes mediated by photons or high-frequency ultrasound. Anticancer effects can be obtained by using high-frequency ultrasound and laser in CCF–HIONP presence. It is suggested that high-frequency ultrasound therapy, in conjunction with light photon irradiation, is a very effective anticancer treatment. Based on our research, CCF–HIONP shows great promise as a new sensitizer and as a useful drug for high-frequency ultrasound–photodynamic therapy (HIFU–SPDT).

Conclusion

The current study resulted in significant results by using chia, cress and flax conjugated hematite iron oxide nanoparticles (CCF–HIONP) as a sensitizer delivery system for high-frequency sono-photodynamic treatment (HIFU–SPDT) to treat lung cancer in vitro (A549 cell line) and in vivo (benzo[a]pyrene induced mice), revealing promising cancer treatment outcomes. Furthermore, CCF–HIONP is a promising cancer therapeutic option due to its numerous benefits, such as excellent bioavailability and low systemic toxicity. Furthermore, the combination of CCF–HIONP@IRL@HIFU–US has opened up a plethora of anticancer medication alternatives for the effective treatment of lung cancer.

Recommendation

The present work manifested that chia, cress and flax conjugated hematite iron oxide nanoparticles (CCF–HIONP) as a new sensitizer in combination with high-frequency sono-photo-dynamic (HIFU–SPDT) promising therapeutic strategy that needs more confirmation for the treatment of lung cancer. Further study methods that securely apply this leading method and technology to humans and track changes in different biophysical and/or biochemical indices are highly recommended.

Abbreviations

ALT	Alanine aminotransferase
AST	Aspartate aminotransferase
BBN	N-butyl-N-(4-hydroxybutyl) nitrosamine
CAT	Catalase
CCF-HIONP	Chia, cress and flax conjugated hematite iron oxide nanoparticles
$FeCl_3.6H_2O$	Ferric chloride hexahydrate
GPx	Glutathione peroxidase
GR	Glutathione reductase
GSH	Reduced glutathione
GST	Glutathione-S-transferase
HIFU–SDT	High-frequency sono-dynamic treatment
HIFU–SPDT	High-frequency sono-photo-dynamic therapy
HIFU–US	High-frequency ultrasound

IRL	Infra-red laser
LCA	Lung cancer
MDA	Malondialdehyde
NaOH	Sodium hydroxide
PDT	Photodynamic therapy
ROS	Reactive oxygen species
SOD	Superoxide dismutase
SRB	Sulforhodamine B
TAC	Total antioxidant capacity

Supplementary Information

The online version contains supplementary material available at https://doi.org/10.1186/s12645-024-00282-2.

Additional file 1.

Acknowledgements
Not applicable.

Author contributions
"All authors contributed to the writing of this manuscript, and all contributors approved the final version of the manuscript. S.A.A.E. design the work and wrote the main manuscript text, D.F.M.Z. prepared figures, H.M.M. participated in interpretation of results, A.S.M.S. participated in statistical analysis, S.M.E.K. participated in result analysis interpretation and writing, M.K.E.D.N. participated in discussion writing. All authors reviewed the manuscript".

Funding
Open access funding provided by The Science, Technology & Innovation Funding Authority (STDF) in cooperation with The Egyptian Knowledge Bank (EKB).

Availability of data and materials
All data generated or analyzed during this study are included in this published article [and its supplementary information files].

Declarations

Ethics approval and consent to participate
The Animal Care and Use Institutional Committee (ALEXU-IACUC; Code No. 01220112911) of Alexandria University granted its certification of ethical guidelines and standards of the animal protocol.

Consent for publication
Not applicable.

Competing interests
The authors declare that they have no competing interests.

Received: 15 June 2024 Accepted: 27 July 2024
Published online: 17 August 2024

References

Abd El-Kaream SA (2019) Biochemical and biophysical study of chemopreventive and chemotherapeutic anti-tumor potential of some Egyptian plant extracts. Biochem Biophys Rep 18:100637
Abd El-Kaream SA, Abd Elsamie GH, Abd-Alkareem AS (2018) Sono-photodynamic modality for cancer treatment using bio-degradable bio-conjugated sonnelux nanocomposite in tumor-bearing mice: activated cancer therapy using light and ultrasound. Biochem Biophys Res Commun 503:1075
Abd El-Kaream SA, Abd Elsamie GH, Abbas AJ (2019a) Sono and photo sensitized gallium-porphyrin nanocomposite in tumor-bearing mice: new concept of cancer treatment. Am J Nanotechnol Nanomed 2:5
Abd El-Kaream SA, Abd Elsamie GH, Metwally MA, Almamoori AYK (2019b) Sono and photo stimulated chlorine e6 nanocomposite in tumor-bearing mice: upcoming cancer treatment. Radiol Med Diag Imag 2:1
Abd El-Kaream SA, Abd Elsamie GH, Isewid GA (2019c) Laser and ultrasound activated photolon nanocomposite in tumor-bearing mice: new cancer fighting drug-technique. Arch Oncol Cancer Ther 2:1
AbdEl-Kaream S, Mohamed HA, El-Kholey SM, AbdRakhey MMM, Elkallaf AMS, Soliman ASM et al (2023) Ultrasound allied laser sono-photobiomodulation activated nano-curcumin: up-and-coming selective cancer cell killing modality. BioNanoSci 13:49–65
Abdulrahman JM, Abd Elsamie GH, Al-rawi RAA, Abd El-kaream SA (2020) Anti-tumor synergistic activity of nano-chlorophyll with sonophotodynamic on Ehrlich ascites carcinoma in mice. Zanco J Med Sci 24:132
Abu Rakhey MMM, El-Kaream SAA, Daoxin M (2022) Folic acid conjugated graphene oxide graviolananoparticle for sonophotodynamic leukemia treatment: up-to-date cancer treatment modality. J Biosci Appl Res 8:28–45
Aebi H (1984) Catalase in vitro. Methods Enzymol 105:121–126

Asha S, Girija D (2011) Benzo[a]pyrene induced liver and kidney cancer in SWISS albino mice. Res Pharmacy 1:22–27
Azene M, Habte K, Tkuwab H (2022) Nutritional, health benefits and toxicity of underutilized garden cress seeds and its functional food products: a review. Food Prod Process Nutr 4:33
Bray F, Ferlay J, Soerjomataram I, Siegel RL, Torre LA, Jemal A (2018) Global cancer statistics 2018: GLOBOCAN estimates of incidence and mortality worldwide for 36 cancers in 185 countries. CA Cancer J Clin 68:394–424
Buckner AL, Buckner CA, Montaut S, Lafrenie RM (2019) Treatment with flaxseed oil induces apoptosis in cultured malignant cells. Heliyon 5:e02251
Burtis CA, Ashwood ER, Bruns DE (2008) Tietz fundamentals of clinical chemistry, 6th edn. Elsevier Saunders Company, St Louis, pp 323–325
Carrasco-Esteban E, Domínguez-Rullán JA, Barrionuevo-Castillo P, Pelari-Mici L, Leaman O, Sastre-Gallego S et al (2021) Current role of nanoparticles in the treatment of lung cancer. J Clin Transl Res 7:140–155
Dardeer AGE, Hussein NG, Abd El-Kaream SA (2021a) New impacts of garcinia Cambogia as Sono/photosensitiser on Ehrlich ascites carcinoma bearing mice. Int J Inf Res Rev 8:7182
Dardeer AGE, Hussein NG, Abd El-Kaream SA (2021b) New Garcinia Cambodia as Sono/Photosensitizer on ehrlich ascites carcinoma bearing mice in presence of dieldrin pesticide as an environmental pollutant. Int J Innov Sci Res 10:1583
De Silva SF, Alcorn J (2019) Flaxseed lignans as important dietary polyphenols for cancer prevention and treatment: chemistry, pharmacokinetics, and molecular targets. Pharmaceuticals 12:68
Deng C, Dang F, Gao J, Zhao H, Qi S, Gao M (2018) Acute benzo[a]pyrene treatment causes different antioxidant response and DNA damage in liver, lung, brain, stomach and kidney. Heliyon 4:00898
Draper HH, Hadley M (1990) Malondialdehyde determination as index of lipid peroxidation. Methods Enzymol 186:421–431
Du X, Li D, Wang G, Fan Y, Li N, Chai L et al (2021) Chemoprotective effect of atorvastatin against benzo(a)pyrene-induced lung cancer via the inhibition of oxidative stress and inflammatory parameters. Ann Transl Med 9:355
El Makawy AI, Abdel-Aziem SH, Mohammed SE, Ibrahim FM, Abd EL-kader HA, Sharaf HA et al (2024) Exploration of tumor growth regression of quinoa and chia oil nanocapsules via the control of PIK3CA and MYC expression, anti-inflammation and cell proliferation inhibition, and their hepatorenal safety in rat breast cancer model. Bull Natl Res Cent 48:7
El Makawy AI, Mabrouk DM, Mohammed SE, Abdel-Aziem SH, El-Kader HAA, Sharaf HA et al (2022) The suppressive role of nanoencapsulated chia oil against DMBA-induced breast cancer through oxidative stress repression and tumor genes expression modulation in rats. Mol Biol Rep 49:10217–10228
Habing WH, Pabst MJ, Jakoby WB (1974) Glutathione S-transferases. The first enzymatic step in mercapturic acid formation. J Biol Chem 249:7130–7139
Han Y, Zheng Z, Liu F, Tian Y, Bi L, Zhang S (2020) Antineoplastic potential of eupatilin against benzo[a]pyrene-induced lung carcinogenesis. Pharmacogn Mag 16:843
Hochhegger B, Alves GR, Irion KL, Fritscher CC, Fritscher LG, Concatto NH et al (2015) PET/CT imaging in lung cancer: indications and findings. J Bras Pneumol 41:264–274
Hu X, Geetha RV, Surapaneni KM, Veeraraghavan VP, Chinnathambi A, Alahmadi TA et al (2021) Lung cancer induced by Benzo(A)Pyrene: ChemoProtective effect of sinapic acid in swiss albino mice. Saudi J Biol Sci 28:7125–7133
Ibrahim MM, Mounier MM, Bekheet SA (2023) Targeting apoptotic anticancer response with natural glucosinolates from cell suspension culture of Lepidium sativum. J Genet Eng Biotechnol 21:53
Jasim AA, Abdulrahman JM, Abd El-kaream SA, Hosny G (2019) Biochemical and pathological evaluation of the effectiveness of nano-targeted sono-photodynamic therapy in breast cancer. J Biosci Appl Res 5:18
Justus CR, Leffler N, Ruiz-Echevarria M, Yang LV (2014) In vitro cell migration and invasion assays. J vis Exp 88:51046
Kamaraj S, Ramakrishnan G, Anandakumar P, Jagan S, Devaki T (2009) Antioxidant and anticancer efficacy of hesperidin in benzo(a)pyrene induced lung carcinogenesis in mice. Invest New Drugs 27:214–222
Kim JA, Åberg C, Salvati A, Dawson KA (2012) Role of cell cycle on the cellular uptake and dilution of nanoparticles in a cell population. Nat Nanotechnol 7:62–68
Kim M, Jee SC, Sung JS (2024) Hepatoprotective effects of flavonoids against Benzo[a]Pyrene-induced oxidative liver damage along its metabolic pathways. Antioxidants 13:180
Ko EC, Raben D, Formenti SC (2018) The integration of radiotherapy with immunotherapy for the treatment of non-small cell lung cancer. Clin Cancer Res 24:5792–5806
Kozower BD, Larner JM, Detterbeck FC, Jones DR (2013) Special treatment issues in non-small cell lung cancer: diagnosis and management of lung cancer: American college of chest physicians evidence-based clinical practice guidelines. Chest 143:369S-S399
Kulczyński B, Kobus-Cisowska J, Taczanowski M, Kmiecik D, Gramza-Michałowska A (2019) The chemical composition and nutritional value of chia seeds-current state of knowledge. Nutrients 11:1242
Lei H, Pei Z, Jiang C, Cheng L (2023) Recent progress of metal-based nanomaterials with anti-tumor biological effects for enhanced cancer therapy. Exploration (beijing) 3:20220001
Marklund S, Marklund G (1974) Involvement of the superoxide anion radical in the autoxidation of pyrogallol and a convenient assay for superoxide dismutase. Eur J Biochem 47:469–474
Merkher Y, Kontareva E, Alexandrova A, Javaraiah R, Pustovalova M, Leonov S (2023) Anti-cancer properties of flaxseed proteome. Proteomes 11:37
Mueed A, Deng Z, Korma SA, Shibli S, Jahangir M (2023) Anticancer potential of flaxseed lignans, their metabolites and synthetic counterparts in relation with molecular targets: current challenges and future perspectives. Food Funct 14:2286–2303
Navada KM, Nagaraja GK, D'Souza JN, Kouser S, Ranjitha R, Ganesha A et al (2022) Synthesis of phyto-functionalized nano hematite for lung cancer suppressive activity and paracetamol sensing by electrochemical studies. Process Biochem 123:76–90
Nithya G, Santhanasabapathy R, Vanitha MK, Anandakumar P, Sakthisekaran D (2023) Antioxidant, antiproliferative, and apoptotic activity of thymoquinone against benzo(a)pyrene-induced experimental lung cancer. J Biochem Mol Toxicol 37:23230

Noguchi M, Hirata N, Tanaka T, Suizu F, Nakajima H, Chiorini JA (2020) Autophagy as a modulator of cell death machinery. Cell Death Dis 11:517
Nurhayati T, Iskandar F, Abdullah M, Khairurrija K (2013) Syntheses of hematite (α-Fe2O3) nanoparticles using microwave-assisted calcination method. Mater Sci Forum 737:197–203
Omidian K, Rafiei H, Bandy B (2017) Polyphenol inhibition of benzo[a]pyrene-induced oxidative stress and neoplastic transformation in an in vitro model of carcinogenesis. Food Chem Toxicol 106:165–174
Pozarowski P, Darzynkiewicz Z (2004) Analysis of cell cycle by flow cytometry. Methods Mol Biol 281:301–311
Qiu G, Xue L, Zhu X, Lu X, Liu L, Wang Z et al (2022) Cetuximab combined with sonodynamic therapy achieves dual-modal image monitoring for the treatment of EGFR-sensitive non-small-cell lung cancer. Front Oncol 12:756489
Rajendran P, Ekambaram G, Sakthisekaran D (2008) Cytoprotective effect of mangiferin on benzo(a)pyrene-induced lung carcinogenesis in swiss albino mice. Basic Clin Pharmacol Toxicol 103:137–142
Rengeng L, Qianyu Z, Yuehong L, Zhongzhong P, Libo L (2017) Sonodynamic therapy, a treatment developing from photodynamic therapy. Photodiagnosis Photodyn Ther 19:159–166
Rice-Evans C, Miller NJ (1994) Total antioxidant status in plasma and body fluids. Methods Enzymol 234:279–293
Rivera MP, Mehta AC, Wahidi MM (2013) Establishing the diagnosis of lung cancer: diagnosis and management of lung cancer: American college of chest physicians evidence-based clinical practice guidelines. Chest J 143:142–165
Sakthivel R, Sheeja MD, Archunan G, Pandima DK (2019) Phytol ameliorated benzo(a)pyrene induced lung carcinogenesis in Swiss albino mice via inhibition of oxidative stress and apoptosis. Environ Toxicol 34:355–363
Sanlier N, Guler SM (2018) The benefits of brassica vegetables on human health. J Human Health Res 1:104–116
Selek S, Koyuncu I, Caglar HG, Bektas I, Yilmaz MA, Gonel A et al (2018) The evaluation of antioxidant and anticancer effects of Lepidium Sativum Subsp Spinescens L. methanol extract on cancer cells. Cell Mol Biol (noisy-Le-Grand) 64:72–80
Shaer N, Al-Abbas N (2022) Potential effect of chia seeds crude extract nanoparticles on Mcf-7 breast cancer cell line. Al-Azhar Int Med J 3:123–127
Shahid A, Chen M, Lin C, Andresen BT, Parsa C, Orlando R et al (2023) The β-blocker carvedilol prevents Benzo(a)pyrene-induced lung toxicity, inflammation and carcinogenesis. Cancers (basel) 15:583
Shen J, Cao S, Sun X, Pan B, Cao J, Che D et al (2018) Sinoporphyrin sodium-mediated sonodynamic therapy inhibits RIP3 expression and induces apoptosis in the H446 small cell lung cancer cell line. Cell Physiol Biochem 51:2938–2954
Siegel RL, Miller KD, Jemal A (2018) Cancer statistics, 2018. CA Cancer J Clin 68:7–30
Soundararajan P, Kim JS (2018) Anti-carcinogenic glucosinolates in cruciferous vegetables and their antagonistic effects on prevention of cancers. Molecules 23:2983–3003
Szasz A (2019) Thermal and non-thermal effects of high frequency ultrasound on living state and applications as an adjuvant with radiation therapy. J Radiat Cancer Res 10:1–17
Thomé MP, Filippi-Chiela EC, Villodre ES, Migliavaca CB, Onzi GR, Felipe KB et al (2016) Ratiometric analysis of Acridine orange staining in the study of acidic organelles and autophagy. J Cell Sci 129:4622–4632
van Tonder A, Joubert AM, Cromarty AD (2015) Limitations of the 3-(4,5-dimethylthiazol-2-yl)-2,5-diphenyl-2H-tetrazolium bromide (MTT) assay when compared to three commonly used cell enumeration assays. BMC Res Notes 8:47
Velli SK, Sundaram J, Murugan M, Balaraman G, Thiruvengadam D (2019) Protective effect of vanillic acid against benzo(a) pyrene induced lung cancer in Swiss albino mice. J Biochem Mol Toxicol 33:22382
Vichai V, Kirtikara K (2006) Sulforhodamine B colorimetric assay for cytotoxicity screening. Nat Protoc 1:1112–1116
Wang Y, Kanneganti T-D (2021) From pyroptosis, apoptosis and necroptosis to PANoptosis: a mechanistic compendium of programmed cell death pathways. Comput Struct Biotechnol J 19:4641–4657
Wlodkowic D, Skommer J, Darzynkiewicz Z (2009) Flow cytometry-based apoptosis detection. Methods Mol Biol 559:19–32
Wu Y, Wang X, Li J, Ma H, Seshadri VD, Wang X (2023) Benzo(A)Pyrene-induced lung cancer: chemo protective effect of coronarin D in Swiss Albino Mice. Appl Biochem Biotechnol 195:1122–1135
Yang G, Liu H, Xu S, Tian Z (2024) Mitigating effect of Matricin against Benzo(a)pyrene-induced lung carcinogenesis in experimental mice model. Comb Chem High Throughput Screen. https://doi.org/10.2174/0113862073273177231130094833
Zhang H, Pan X, Wu Q, Guo J, Wang C, Liu H (2021) Manganese carbonate nanoparticles-mediated mitochondrial dysfunction for enhanced sonodynamic therapy. Exploration (beijing) 1:20210010

Publisher's Note